Sustainable Energy & Fuels

Interdisciplinary research for the development of sustainable energy technologies

Accepted Manuscript

This article can be cited before page numbers have been issued, to do this please use: J. Xie, S. Sankarasubramanian and V. Ramani, *Sustainable Energy Fuels*, 2026, DOI: 10.1039/D5SE01171J.

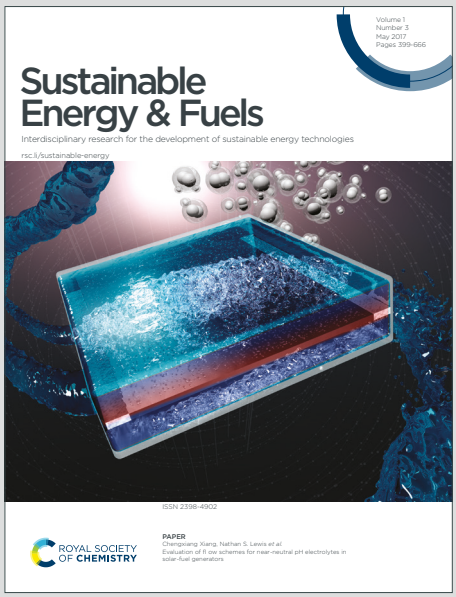

ROYAL SOCIETY OF CHEMISTRY

rsc.li/sustainable-energy

View Article Online
DOI: 10.1039/D5SE01171J

Asymmetric Electrode Configurations Enhance Operating Power Density and Energy Efficiency of the Aqueous, Electrode-decoupled Titanium-Cerium Redox Flow Battery

Jing Xie[a], *Shrihari Sankarasubramanian*[b,c], *Vijay Ramani*[a,]*

[a] Department of Energy, Environmental and Chemical Engineering, Washington University in St. Louis, St. Louis, MO 63130, USA

[b] Department of Biomedical Engineering and Chemical Engineering, The University of Texas at San Antonio, San Antonio, TX 78249, USA.

[c] Department of Mechanical, Aerospace and Industrial Engineering, The University of Texas at San Antonio, San Antonio, TX 78249, USA.

*Corresponding author

Author e-mails: xiejing@wustl.edu (J. Xie); shrihari.sankarasubramanian@utsa.edu (S. Sankarasubramanian); ramani@wustl.edu (V. Ramani)

Abstract

Redox flow batteries (RFBs), with decoupled scaling in energy and power, are an attractive solution for grid scale energy storage. Given the low margins and extreme price sensitivity of electricity supply, it is critically important for RFBs to reduce capital and operating costs. Improving the operating power density and energy efficiency of the RFB is a pathway towards lowered costs but achieving simultaneous improvements in both parameters is hampered by the fact that they are typically inversely correlated. This study demonstrates a 50% improvement in operating power density of an aqueous, electrode-decoupled Titanium-Cerium RFB without loss of energy efficiency through electrode engineering driven by fundamental investigations of charge-transfer kinetics at the Ti and Ce electrodes. Exploiting the significant difference in reaction kinetics between the Ti and Ce actives, the interfacial area and surface functionalization (affecting electrode-electrolyte contact angles and kinetics of charge transfer) of the electrode were

View Article Online
DOI: 10.1039/D5SE01171J

optimized to increase operating power while reducing overall cell resistance. This resulted in increasing operating current density of a Ti-Ce RFB from 100 mA cm^{-2} to 150 mA cm^{-2} while sustaining ~70% energy efficiency over 80 h and 100 cycles. Notably, this study shows the key role played by the rate limiting electrode and the effect of electrode surface area in improving its performance. Overall, this study offers a template to significantly improve the overall performance of kinetically limited aqueous RFBs without catalysts or electrolyte reformulation.

Keywords: redox flow batteries, carbon paper, methanesulfonic acid, large-scale energy storage

1. Introduction

The development of large-scale, robust, and cost-effective energy storage systems, such as rechargeable batteries is a critical component of transitioning to sustainable but intermittent energy sources such as solar and wind.[1-4] Among them, redox flow batteries (RFBs) are a promising candidate because of their unique advantage: the energy capacity storage and output power density are decoupled, allowing for independent scale-up, and thus great design flexibility.[5-7] Among the different types of RFBs, all vanadium ones (VRFBs), introduced in the 1980s, have been extensively studied and commercialized.[8] The use of vanadium redox couples on both sides (enabled by the prevalence of multiple readily soluble oxidation states of V) mitigates active species crossover (a common failure mode and source of performance loss) and provides a unique operational advantage.[9] However, the scaling up of VRFBs is limited by the high cost of vanadium and relatively low standard potential (1.26 V vs. standard hydrogen electrode (SHE)), making it difficult to meet cost targets for grid scale energy storage.[10] Thus, moving away from

View Article Online
DOI: 10.1039/D5SE01171J

vanadium as the active species is a potential solution but a key barrier to moving away from the VRFB is the fact that few other elements in the periodic table exhibit vanadium ion's characteristic of being soluble at more than 2 oxidation states. Alternately, techno-economic analysis (TEA) has shown that increasing the operating voltage and operating current density (translating to the operating power density) is critically important for reducing capital costs.[11] The capital costs have been found to be a strongly non-linear function of both operating voltage and operating current density, with capital costs for 6 different flow battery chemistries falling by 70%-90% when the operating current density is increased from 10 mA cm^{-2} to >100 mA cm^{-2}.[11-12] TEA indicated capital cost reductions of ~50% for RFBs with elemental actives (all-V, Zn-Br) when the operating voltage increased from 0.6 V to 1.2 V.[11] Thus, increasing RFB operating current density to >100 mA cm^{-2} and the operating voltage to >1 V is expected to dramatically reduce capital costs. The levelized cost of storage (LCOS) has been shown to be strongly coupled to the capital cost and is further affected by cycle duration (with some studies showing 4–10-hour cycles being the optimum).[13] But alternatives to VRFBs considered in the studies referenced above suffer from their own issues such as crossover of active species, toxicity (Br), phase change/plating-stripping reactions leading to dendrite formation (Zn, Pb etc.) and unwanted side reactions (evolution of hydrogen or oxygen). The titanium-cerium RFB, a relatively new chemistry first reported in 2019 solves these chemistry problems and has been shown to meet all DOE cost targets.[14-15] Particularly, the Ti-Ce RFB employs a selective anion exchange membrane (AEM) separator that significantly impedes the crossover of the redox active cations, making it an "electrode-decoupled" system. In this study, starting with an already inexpensive RFB chemistry (titanium-cerium (Ti-Ce)), we demonstrate RFB electrode engineering methods that can achieve significant

View Article Online
DOI: 10.1039/D5SE01171J

improvements in operating power density by increasing current density with minimal associated increase in overpotential.[14-15]

The Ti-Ce RFB is a relatively new system that has been shown to both meet DOE cost targets and has the ability to be cycled diurnally.[14-15] The Ce redox couple has been examined as a possible active for RFBs due to two advantages: a high standard potential (1.61 V vs. SHE) and abundant geographical availability with relatively low cost.[16-17] The major challenge of deploying Ce redox couple in RFBs is that Ce solubility is limited in sulfuric acid (H_2SO_4), a typical supporting electrolyte. In H_2SO_4, Ce solubility has been reported to be below 0.5 M and decreases as the concentration of H_2SO_4 increases.[18] As an alternative, methanesulfonic acid (MSA) has been shown to increase Ce solubility significantly with an inverse relationship between solubilities of Ce(III) and Ce(IV) as a function of MSA concentration.[19] Ce redox couple utilizing MSA as the supporting electrolyte has been used in multiple RFBs, including Zn-Ce,[20] Pb-Ce,[21] and V-Ce.[22] Ti and its alloys have been widely utilized in medical treatment,[23] aerospace,[24] and automobiles.[25] In RFBs, Ti has been decorated onto electrodes or membranes as a catalyst to promote the performance of VRFBs and as the redox active species in some RFB systems.[26-28] In fact, the abundance and production rate of Ti is about 50 and 100 times that of V, respectively, contributing to a market price that is $1/10^{th}$ of V.[28] Moreover, a standard potential of 0.19 V vs. SHE makes the Ti redox couple a good candidate for RFBs as it is less prone to hydrogen evolution reaction (HER) during the operation of RFBs. In recent years, Ti-based RFBs, such as Fe-Ti[29] and Mn-Ti[30] systems have been proposed and studied. We have combined the Ti and Ce redox couples to develop a fully dissolved (i.e., no phase change or plating/stripping process) RFB that leverages the inherent advantages of both couples.

View Article Online
DOI: 10.1039/D5SE01171J

Starting with a cost effective RFB chemistry that consists of earth abundant elemental actives, we focused on increasing the activity of the electrodes while decreasing their contribution to overall RFB cell resistance so as to achieve higher operating current density without increasing the overpotential. Given that the electroactive species in a RFB is typically dissolved in the electrolyte, the electron transfer process occurs on high surface area, porous electrodes that typically avoid using catalysts to keep down the cost. Carbon felt (CF) is amongst the most commonly utilized electrode material in RFBs due to its high surface area, good stability in an acidic environment, and high conductivity.[31] Carbon paper (CP) has also been used as an electrode candidate but the combination of significantly lower porosity (compared to CF) and the associated increase in pressure drop has meant that most existing studies on CP focus on VRFBs where the reduction in ohmic losses enabled by the thinner CP electrode offers a significant advantage.[32] Typically, carbon electrodes are pretreated before RFB operation to enhance reactant transport and create surface functional groups that aid charge transfer kinetics, and heat treatment is a convenient method that has been extensively studied.[33-34] It has been recognized that significant performance improvements can be achieved by varying the electrode surface area, thickness and pre-treatment protocols. For example, Agar *et al.* and Li *et al.* investigated the performance-limiting side of VRFBs by applying CF with different pretreatment methods on the positive and negative sides and concluded that the performance of VRFBs was limited by the negative side.[35-36] Wei *et al.* showed that the electrochemical activity for the positive and negative sides of VRFBs was promoted by carbon nanofibers decorated with carbon nanotubes and Bi-based compounds, respectively.[37] Similarly, Jing *et al.* embedded tungsten and antimony on positive and negative carbon nanofibers, respectively, to achieve the highest performance of VRFBs.[38] Lu *et al.* provided evidence from a two-dimensional, transient model simulation that

View Article Online
DOI: 10.1039/D5SE01171J

the performance of VRFBs could be further improved by applying a higher compression ratio of positive electrodes.[39] Nevertheless, the focus of a majority of these studies has been the impact on a particular RFB performance parameter, oftentimes to the detriment of other parameters. These studies improve the performance by (i) reducing ohmic losses by employing thinner electrodes or (ii) by decreasing activation polarization losses by electrode surface treatment and catalysts. It is challenging to employ both approaches in tandem as thinner electrodes have lower total surface area and thus reduce overall rate while surface treatment of the electrodes or use of catalysts can reduce electrical conductivity and increase pressure drop, thereby increasing ohmic losses. Our study shows how fundamental studies of electrode kinetics and electrode wetting can be used to enable simultaneous decreases in activation polarization losses and ohmic polarization losses, and this was achieved in an electrode decoupled RFB where the two electrodes exhibit very different redox behaviors. Leveraging and extending the insights from these studies, we demonstrate a Ti-Ce RFB with an asymmetric electrode configuration successfully operated at 150 mA cm^{-2}, delivering an energy efficiency (EE) of 67.8% and capacity retention of 93%. We present a roadmap for the use of fundamental electrochemical investigations (kinetics and transport studies using cyclic voltammetry) to downselect appropriate carbon electrodes for RFBs with the aim of maximizing cell level performance. The approach demonstrated with Ti-Ce RFBs can be equally applied to other systems.

View Article Online
DOI: 10.1039/D5SE01171J

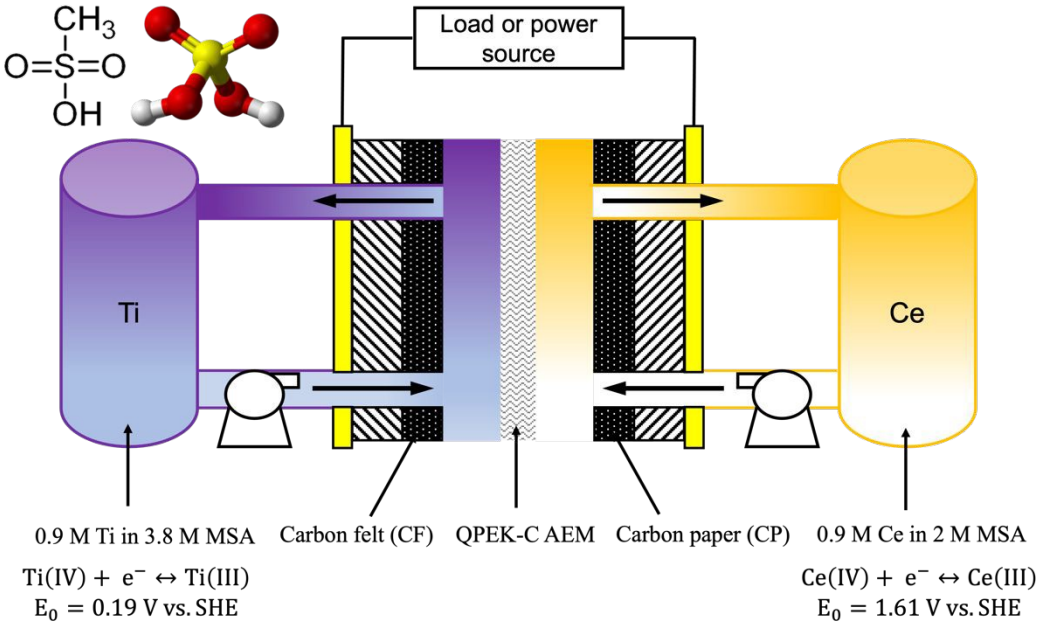

Scheme 1. Schematic illustration of Ti-Ce RFB with asymmetric electrode configuration. The separator is a custom anion exchange membrane (AEM) whose synthesis and characterization is detailed elsewhere.[70-71]

2. Results and Discussion

2.1 Effect of heat treatment on CP and CF

In order to confirm the potential modifications to both carbon electrodes brought by heat treatment, scanning electron microscope (SEM) was used to examine the morphology of CP and CF before and after heat treatment, as presented in **Figure 1**. CP was found to be composed of rigid and straight fibers, and no significant difference could be observed between pristine CP and heat-treated CP (HT CP). On the contrary, CF was made of soft and curvy fibers, and the surface of CF fibers became rougher and more porous after heat treatment, indicating significant surface modification and potential increase in surface area. Energy dispersive X-ray (EDX) spectra showed that the oxygen content remained mostly unchanged between CP and HT CP while a significant increase in surface oxygen was detected on CF post heat treatment) (See **Table 1**). This

View Article Online
DOI: 10.1039/D5SE01171J

correlation between surface morphology and surface oxygen content agrees with prior results showing that the thermal treatment oxidizes the carbon surface.[34] Results of surface investigations using X-ray photoelectron spectroscopy (XPS) are depicted in **Figure 2** (XPS survey spectra depicted in **Figure S1**). The C1s data shows minimal changes in case of CP while the percentage of C-C was found to decrease and the percentage of C=C increased in case of CF, indicating an increase in C defect sites on the surface necessitating the formation of unsaturated C=C bonds. This was coupled with an increase in C-OH and C=O groups, indicating the presence of at least 3 different potential reaction sites on the surface. Oxygen functional groups were found to increase in percentage on HT CF, while there was not much difference between the XPS results of CP and HT CP. Interestingly, ether groups increased after thermal treatment, indicating that some of the C defect sites were being occupied by O. The ratio between alcohol groups and carbonyl groups inverted following thermal treatment, indicating oxidation of the alcohol groups to the corresponding carboxyl group. Given the difference in electrochemical activity between surface alcohol and carboxyl groups, the ratio between these groups would significantly affect the activity of a given carbon electrode and this explains the impact of thermal treatment duration on carbon electrode activity. The change of CF by heat treatment was consistent with previous studies that applied CF as electrodes in VRFBs.[33, 36, 40] The percentages of various functional groups in different samples as measured by XPS is listed in **Table 2**. It was also proposed by these studies that the oxygen functional groups could work as catalytic sites to enhance the kinetics of vanadium redox reactions, and similar positive effects on Ti reaction were found in our study, which will be discussed further. The number of studies on the effects of heat treatment on CP is still limited, possibly because CP is not used as widely as CF. One previous study pointed out that the effect of

View Article Online
DOI: 10.1039/D5SE01171J

thermal treatment on CP was nuanced and controlled by several factors (e.g., microstructure and surface chemistry).[34]

Table 1 Atomic ratios (%) of carbon and oxygen from EDX

Elements	Pristine CP	HT CP	Pristine CF	HT CF
C	99.6 ± 0.1	99.6 ± 0.1	99.9 ± 0.0	95.8 ± 0.7
O	0.4 ± 0.0	0.4 ± 0.1	0.1 ± 0.0	4.2 ± 0.4

Table 2 Percentage of different chemical bonds from XPS

		Pristine CP	HT CP	Pristine CF	HT CF
C1s	Total	96.8 ± 0.2	98.5 ± 0.1	96.7 ± 0.2	90.5 ± 0.6
	C=C	76.2 ± 6.8	81.6 ± 5.0	51.4 ± 4.9	78.0 ± 5.9
	C-C	13.6 ± 4.2	17.3 ± 3.6	40.0 ± 5.2	9.8 ± 2.2
	C-OH	9.5 ± 3.3	1.1 ± 0.5	8.6 ± 2.5	10.1 ± 1.6
	C=O	0.7 ± 0.1	0.1 ± 0.1	0.0 ± 0.1	2.1 ± 0.9
O1s	Total	2.8 ± 0.1	1.5 ± 0.0	2.6 ± 0.1	8.6 ± 0.5
	Carbonyl	2.5 ± 0.4	0.0 ± 0.1	0.0 ± 0.1	2.8 ± 1.2
	Alcohol	39.2 ± 3.8	53.0 ± 4.8	52.3 ± 5.3	37.7 ± 3.6
	Carboxyl	58.3 ± 2.4	47.0 ± 3.1	47.7 ± 3.4	59.5 ± 5.2

View Article Online
DOI: 10.1039/D5SE01171J

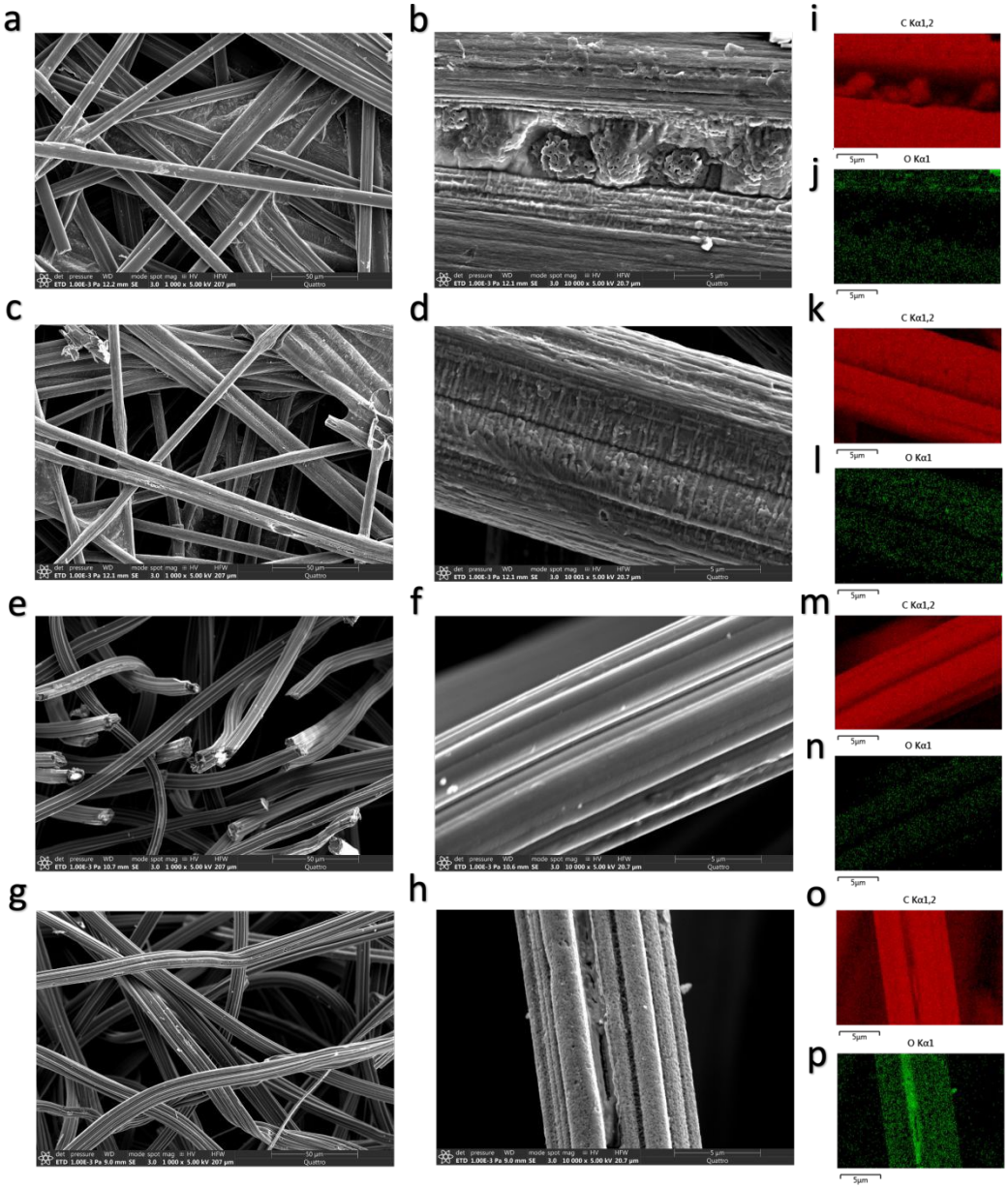

176

177 **Figure 1.** SEM/EDX of pristine CP (a, b, i, j), HT CP (c, d, k, l), pristine CF (e, f, m, n), and HT
178 CF (g, h, o, p).

179

View Article Online
DOI: 10.1039/D5SE01171J

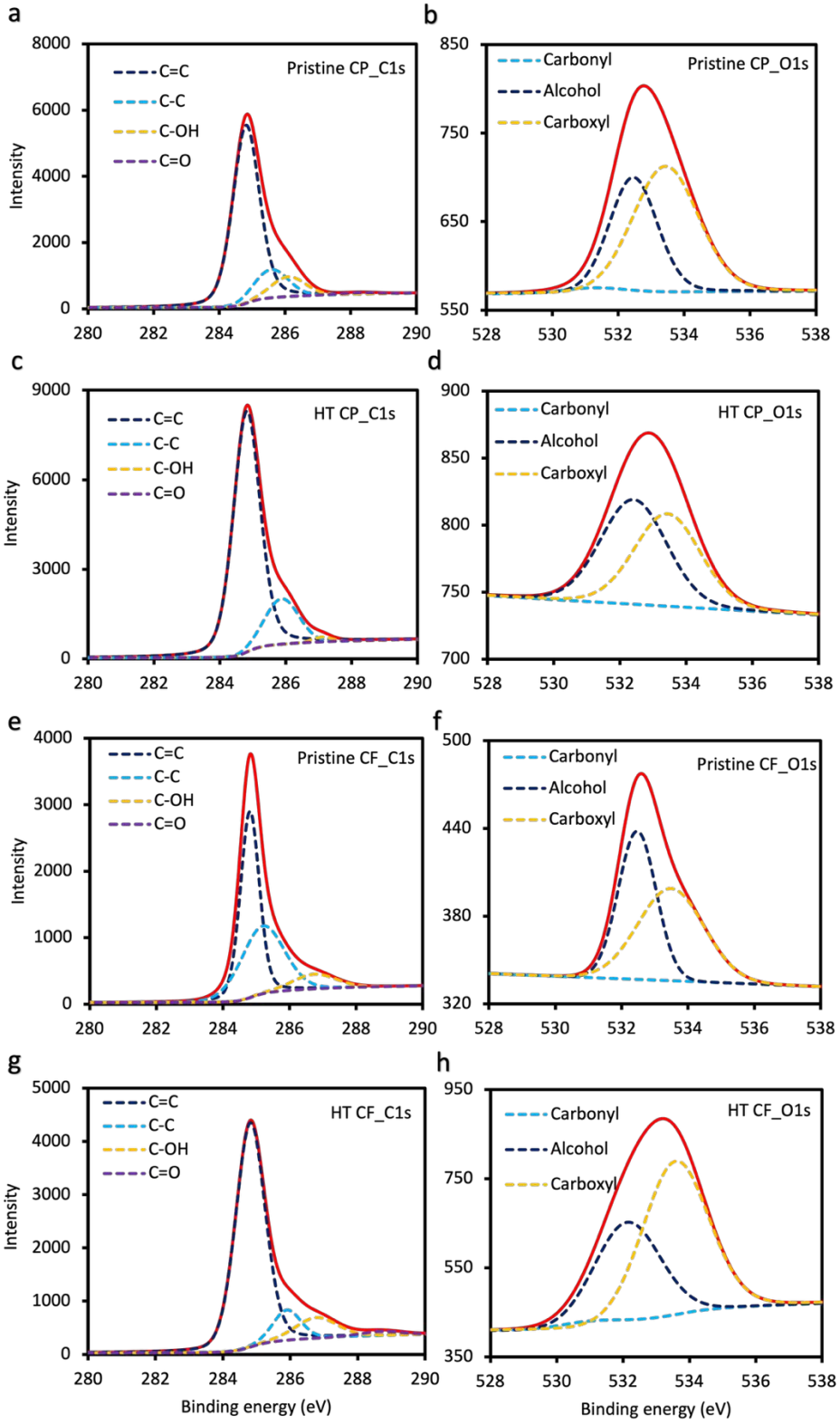

Figure 2. XPS of pristine CP (a and b), HT CP (c and d), pristine CF (e and f), and HT CF (g and h).

View Article Online
DOI: 10.1039/D5SE01171J

2.2 Effect of Thermal Treatment on Electrode-Electrolyte Interaction

During the operation of RFBs, electrolytes flow into the cell to contact the electrode, where the reactions take place, and high hydrophilicity is desirable to reduce mass transfer resistance.[32] The effect of electrode thermal treatment on the interfacial contact between the Ti and Ce electrolyte and the CF and CP electrodes was characterized through contact angle measurements using a Goniometer. The contact angle was measured using ImageJ 1.54g, Java 1.8.0_345 (64-bit) from pictures captured from the goniometer. The side views of Ti and Ce electrolyte droplets on carbon electrodes are displayed in **Figure 3**, and the contact angle values are presented in **Table 3**. As seen from **Figure 3**, both the Ti and Ce electrolytes readily spread and were absorbed into the porous electrode bulk in case of CF and HT CF (no apparent bubble is seen visually). The Ce electrolyte also exhibited ready absorption and no apparent bubble formation in case of CP and HT CP. However, the Ti electrolyte formed very obviously shaped droplets on CP, HT CP, and CF, indicating poor wettability. Thus, both the surface functional groups themselves and the characteristics of the electrolyte determine interfacial contact. The excellent hydrophilicity exhibited by HT CF with both Ce and Ti electrolytes was ascribed to the oxygen functional groups,[41] which was confirmed by SEM/EDX and XPS. Interestingly, all four types of electrodes exhibited good hydrophilicity with Ce electrolyte, indicating that the initial percentage of surface oxygen functional groups was not the only factor. Nikiforidis *et al.* report that a hydrophilic and inhomogeneous surface of CP was created after repetitional cyclic voltammetry (CVs) in a Ce electrolyte.[42] Similar oxidation of the carbon electrodes by Ce(IV) would explain the observed wettability results. Ti is known to form polymer like chains at higher concentrations in solution,[28] thereby affecting the viscosity and diffusion coefficients and this would explain the lack of

View Article Online
DOI: 10.1039/D5SE01171J

wettability on unfunctionalized surfaces. As reported in Ahmed *et al.*, the dynamic viscosity of Ti electrolytes in sulfuric acid has been found to increase from 1cP to 2.4cP when the H_2SO_4 concentration increased from 0M to 4M while keeping the Ti concentration constant at 0.5M. When the Ti concentration was increased from 0.5M to 5M (with a constant 4M H_2SO_4 concentration) the dynamic viscosity increased from 2.4cP to 7.5cP. Given minimal variation in viscosity when the Ti concentration is kept at 0.5M, we do not anticipate this playing a role in pressure drop, pumping losses etc.[72] These results indicated that HT CF is the optimal electrode candidate for the Ti side, but the optimal surface for the Ce side could not be determined on the basis of surface wettability. Furthermore, since both surface characterization and the hydrophilicity test indicated minimal difference between CP and HT CP, we elected to use only CP for further experiments.

Table 3 Contact angles of Ti & Ce electrolyte on CP & CF

Electrodes	Ti	Ce
Pristine CP	109.8° ± 5.6°	a)
Pristine CF	113.6° ± 7.8°	a)
HT CP	98.8° ± 4.0°	a)
HT CF	a)	a)

a) found to spread and be absorbed on the surface with no discernable bubble formation.

View Article Online
DOI: 10.1039/D5SE01171J

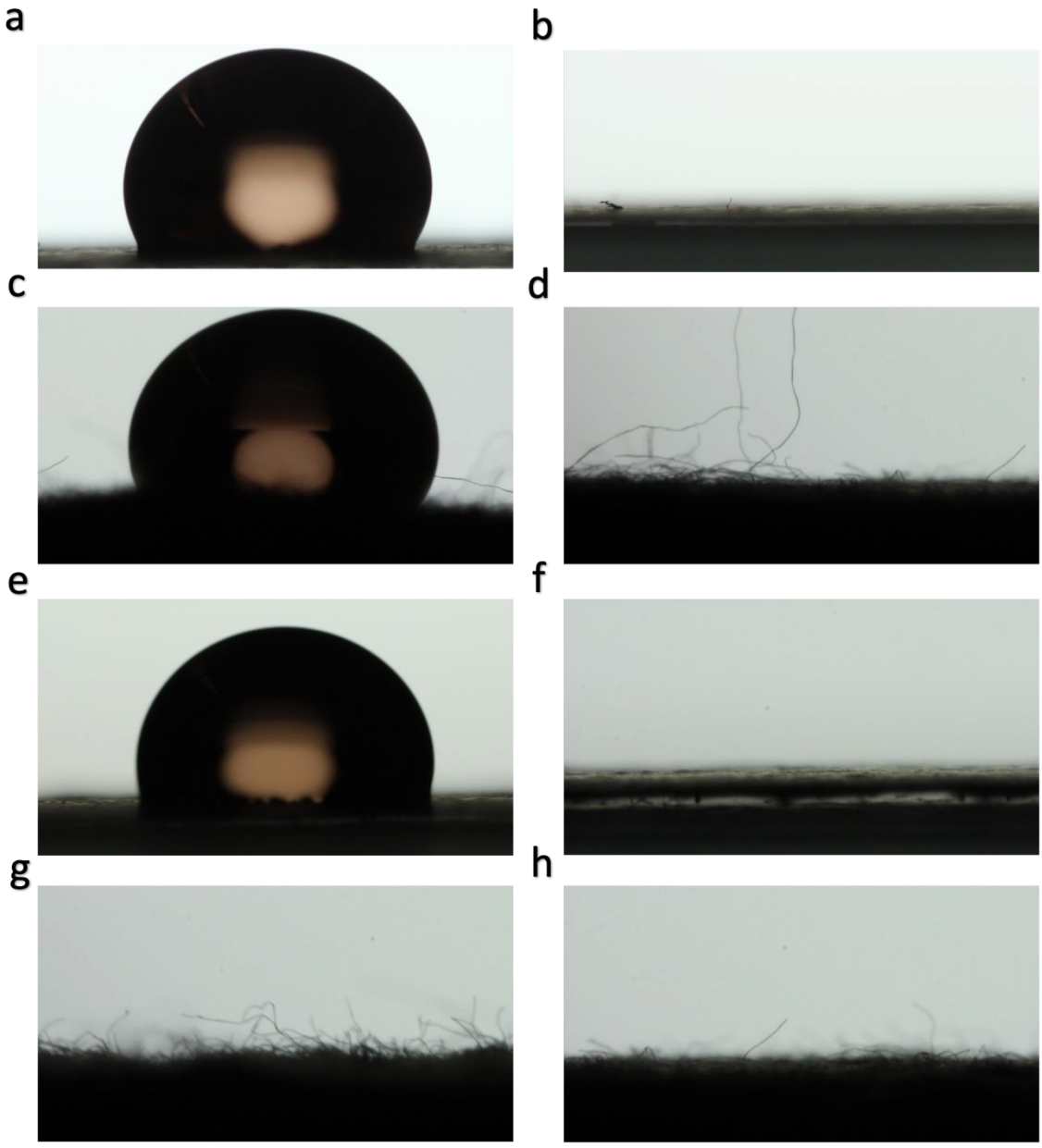

Figure 3. Side views of (a) Ti electrolyte droplet on pristine CP; (b) Ce electrolyte droplet on pristine CP; (c) Ti electrolyte droplet on pristine CF; (d) Ce electrolyte droplet on pristine CF; (e) Ti electrolyte droplet on HT CP; (f) Ce electrolyte droplet on HT CP; (g) Ti electrolyte droplet on HT CF; (h) Ce electrolyte droplet on HT CF.

2.3 Electrochemical behavior of carbon electrodes in Ti and Ce electrolyte

View Article Online
DOI: 10.1039/D5SE01171J

In order to identify the optimum electrode configuration for Ti-Ce RFBs, CVs were recorded utilizing different types of carbon electrodes as the working electrode, as depicted in **Figure 4**. As seen in **Figure 4a**, both Ti reduction and Ti oxidation peaks were observed only on HT CF while pristine CF and CP lacked cathodic peaks, indicating poor activity for Ti reduction. Besides, the anodic peak potentials of pristine CF and CP were much more positive than that of HT CF (0.995 V and 0.798 V respectively vs. 0.075 V), and the corresponding peak currents were more than 20 times smaller than that of HT CF ($5x10^{-4}$ A and $2x10^{-4}$ A respectively vs. 0.012 A), showing HT CF was much more active towards Ti oxidation. This improved activity is ascribed to the surface oxygen functional groups and increased surface roughness (and hence surface area) introduced by heat treatment. This agrees with previous studies in VRFBs,[43] Fe-RFBs,[44] Zn-RFBs,[45] and Cu-RFBs,[46] where electrode heat treatment was found to improve redox kinetics. Based on this, HT CF was selected as the negative electrode in Ti-Ce RFBs. In sharp contrast to its behavior with the Ti redox couple, HT CF showed no redox peaks in case of the Ce electrolyte (except for a gradual increase in current at more anodic potentials, indicating the onset of oxygen evolution) while both anodic and cathodic peaks could be observed on pristine CF and pristine CP. However, each electrode exhibited different but equally desirable behavior: while both the anodic and cathodic peak currents on pristine CF was about 20 times that of CP (0.019 A vs. 0.002 A), indicating higher activity (translating to higher operating current density in the RFB), the peak separation on CP was smaller than that of pristine CF (0.27 V vs. 0.73 V), indicating better reversibility and improved energy efficiency at the RFB cell level.[47] The higher peak current on pristine CF can be partially attributed to the higher surface area of CF than CP. But the fact that HT CF with even higher surface area exhibited negligible Ce redox activity indicated that it was not merely a surface area effect and the lack of oxygen functional groups plays a positive role. The better reversibility on

View Article Online
DOI: 10.1039/D5SE01171J

pristine CP is attributed to the stability of CP in Ce electrolyte since Ce(IV) is a strong oxidizing agent.[48] We hypothesized that the formation of surface oxygen functional groups upon immersion of the pristine CF into the Ce electrolyte led to the relatively higher peak separation observed in the CV. To test this hypothesis, CVs were compared before and after the electrodes were immersed in Ce electrolytes overnight. As depicted in **Figure 4c** and **4d**, both CF and CP degraded in terms of electrochemical performance (lower peak current, increased peak separation). However, the degradation of CF was more significant: the anodic peak was completely lost, and the cathodic peak current decreased by 26.3%. The shift in peak potentials was lower in case of CP, along with no decrease in the anodic current and a 15% decrease in the cathodic current. Thus, CP was established to be more chemically stable to oxidation (in line with the observed lack of surface functionalization observed following thermal oxidation) and was determined to be a better candidate for the electrode of the Ce side, especially during long-term operation.

View Article Online
DOI: 10.1039/D5SE01171J

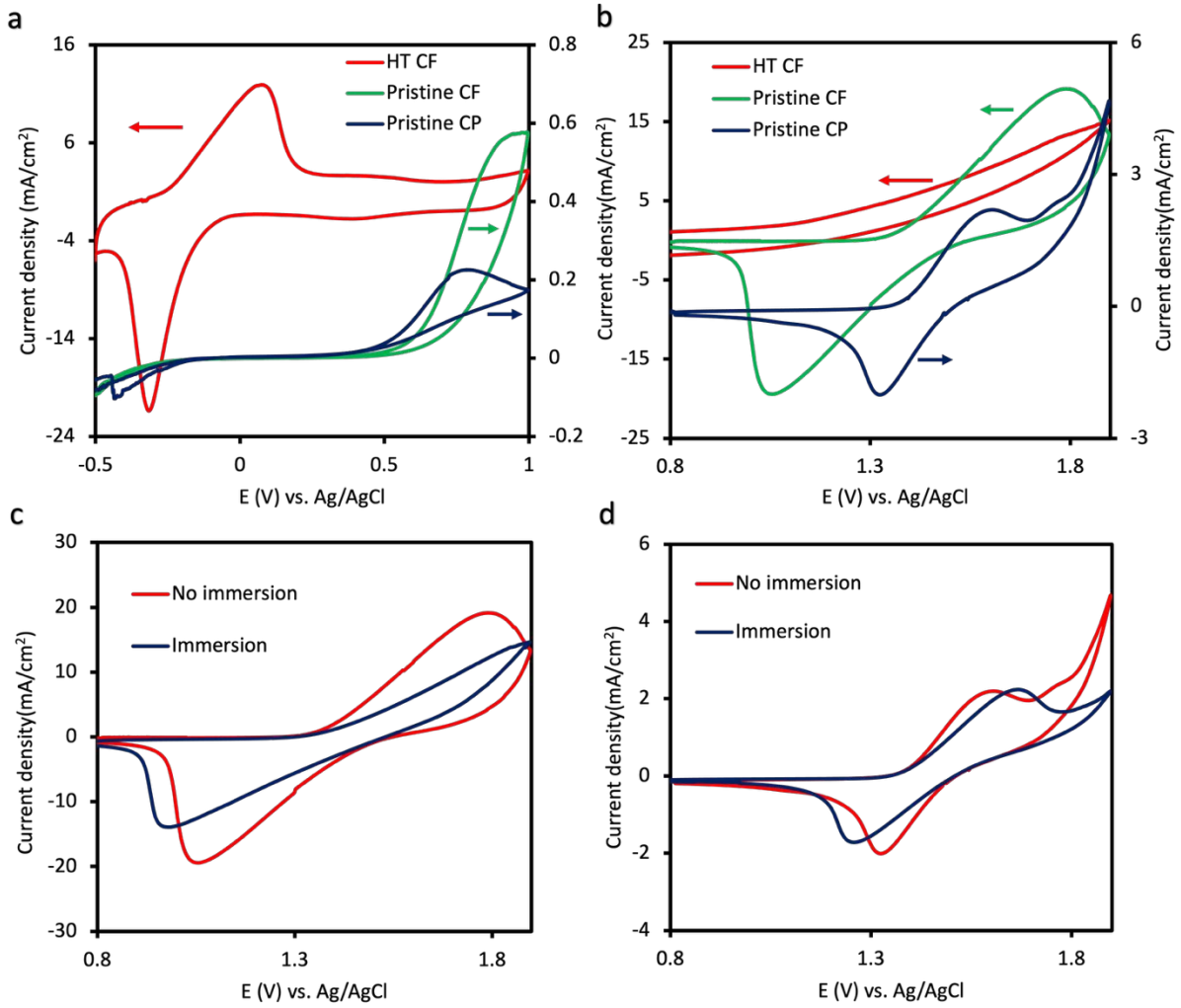

Figure 4. Comparison of electrochemical response with different electrodes in Ti/Ce electrolyte of 50 % SOC at 2.5 mV/s. CVs of HT CF, pristine CF, and pristine CP in a) Ti and b) Ce electrolyte. CVs of c) pristine CF and d) pristine CP before and after being immersed into Ce electrolyte overnight.

The CVs of CP in Ce electrolyte and HT CF in Ti electrolyte at different scan rates are shown in **Figure 5**. The separation of anodic and cathodic peak potentials in **Figure 5a** and **5b** increased with scan rate and was much higher than 59 mV, indicating that both Ti and Ce redox reactions were irreversible.[47] Thus, the Nicholson-Shain (N-S) equation was used to correlate peak currents and scan rates, which is shown below:

View Article Online
DOI: 10.1039/D5SE01171J

$$i_p = (2.99 \times 10^5) n^{3/2} \alpha^{1/2} A C_0 D_0^{1/2} \nu^{1/2} \quad (1)$$

where i_p is the peak current, n is the electron transfer number (1), α is the electron transfer coefficient, A is the surface area of the working electrode (1 cm^2), C_0 is the bulk concentration of active species (0.9 M), D_0 is the diffusion coefficient of active species, and ν is the scan rate.[49-50] Furthermore, the Klinger-Kochi (K-K) equation was used to calculate the standard reaction rate constant, as shown below:

$$k_0 \exp\left[\frac{\alpha n F}{RT}\left(E_p - E^0\right)\right] = 2.18\left[\frac{D\alpha n F \nu}{RT}\right]^{\left(\frac{1}{2}\right)} \quad (2)$$

where k_0 is the standard reaction rate constant, E_p is the potential value at peak current, E_0 is the standard potential, which was obtained from the average of anodic and cathodic peak potential values, R is gas constant (8.314 J mol^{-1} K^{-1}), F is Faraday constant (96485 C mol^{-1}), and T is temperature. Other symbols have the same meaning as in the N-S equation.[51]

View Article Online
DOI: 10.1039/D5SE01171J

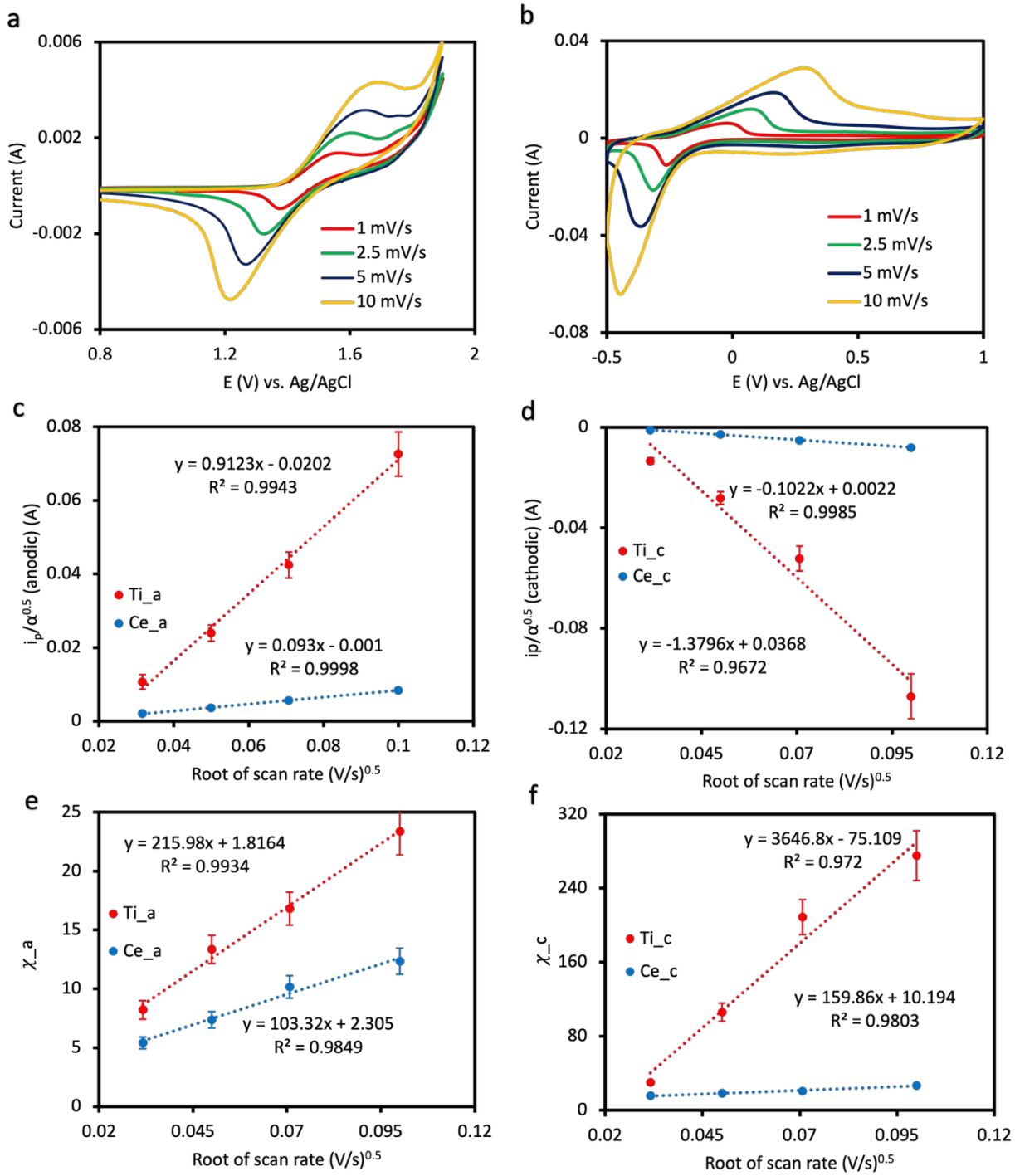

284

285 **Figure 5.** Quantitative analysis of Ti & Ce reaction parameters. CVs of a) CP in Ce electrolyte
286 and b) HT CF in Ti electrolyte at different scan rates. N-S plots of c) anodic and d) cathodic
287 reactions. K-K plots of e) anodic and f) cathodic reactions.

288

View Article Online
DOI: 10.1039/D5SE01171J

Table 4. Electron transfer coefficients of Ti & Ce reactions

Scan rates (mV/s)	Ti_α_a	Ti_α_c	Ce_α_a	Ce_α_c
1	0.334 ± 0.026	0.690 ± 0.037	0.464 ± 0.040	0.755 ± 0.052
2.5	0.294 ± 0.011	0.577 ± 0.034	0.368 ± 0.027	0.536 ± 0.041
5	0.196 ± 0.014	0.485 ± 0.021	0.315 ± 0.016	0.411 ± 0.020
10	0.157 ± 0.009	0.361 ± 0.028	0.270 ± 0.020	0.353 ± 0.029

The traditional N-S plot depicts i_p vs. $\nu^{1/2}$, whose slope is used to calculate D_0. The electron transfer coefficient, α, is usually taken to be 0.5 by convention, as shown in some previous studies.[52-53] However, it should be noted that it is only suitable to assume a value of 0.5 for reversible, elementary single-electron reaction.[47] As mentioned earlier, both Ti and Ce reactions were irreversible, meaning it is unreasonable to do so. In this case, the transfer coefficient, α, was quantitatively calculated by the following equation:[47]

$$\alpha = \frac{1.86RT}{F\left(E_p - E_{\frac{p}{2}}\right)} \quad (3)$$

where $E_{p/2}$ is half-peak potential, which refers to the potential when the current reaches half of i_p. The results of α are listed in **Table 4**, demonstrating that the actual α values were significantly deviating from 0.5 as expected based on the irreversible nature of the reactions. Notably, the α values for the Ti redox couple were found to deviate more from the ideal of 0.5 compared to values measured for the Ti redox couple in H_2SO_4 across a range of supporting electrolyte concentrations.[72] This was attributed to difference in solvation brought about by using MSA as the supporting electrolyte. The application of Equation (3) has been proven to be an effective and

View Article Online
DOI: 10.1039/D5SE01171J

accurate way to determine the charge transfer coefficient[54] and the observation that α values calculated from Equation (3) was inversely correlated with the scan rate was in agreement with that study's conclusions. This phenomenon was understood to be a result of the potential-dependent nature of transfer coefficients at high overpotentials. The Butler-Volmer model assumes an exponential relationship between charge transfer rate and electrode overpotential regardless of how far it is from equilibrium, which is not consistent with the modern understanding of charge transfer.[55-56] Based on this, the original N-S and K-K equations were slightly modified by moving α from right to left side:

$$i_p/\alpha^{1/2} = (2.99 \times 10^5) n^{3/2} A C_0 D_0^{1/2} \nu^{1/2} \quad (4)$$

by defining

$$\chi = exp\left[\frac{\alpha n F}{RT}\left(E_p - E^0\right)\right]/\alpha^{1/2} \quad (5)$$

the K-K equation turns into

$$\chi = \frac{2.18}{k_0}\left[\frac{DnF\nu}{RT}\right]^{\left(\frac{1}{2}\right)} \nu^{1/2} \quad (6)$$

Thus, the diffusion coefficient, D_0, and standard reaction rate constant, k_0, were obtained from the slope of the N-S plot ($i_p/\alpha^{1/2}$ vs. $\nu^{1/2}$) and the K-K plot (χ vs. $\nu^{1/2}$), respectively. The N-S and K-K plots are depicted in **Figure 5**, and the results for D_0 and k_0 are listed in **Table 5**. The diffusion coefficients of Ti on HT CF were more than two orders higher than those of Ce on CP. The porous nature of HT CF was expected to result in the measured diffusion coefficient being an effective diffusion coefficient including the effect of constrained diffusion within the pores of the HT CF. Thus, the fact that the effective diffusion coefficient of Ti is still higher than that of Ce on a much

View Article Online
DOI: 10.1039/D5SE01171J

less porous CP electrode indicates that Ce is transport limited. The measured diffusion coefficients of Ce were more also than one order of magnitude higher than values obtained from some previous studies using dilute Ce solutions (0.01 to 0.2 M) and with sulfuric acid supporting electrolytes.[57-58] The diffusion coefficient of active species is strongly dependent on the concentration and type of supporting electrolyte and thus only broad comparisons of diffusion coefficient trends would be strictly valid when comparing measurements made with electrolytes having different supporting electrolytes. These studies also used a non-porous, planar electrode and thus the difference in calculated diffusion coefficients also reflect the difference between the geometric and electrochemically active surface area (ECSA) of the electrode. The geometric area and ECSA would be very close to each other in the planar model electrodes while the differing significantly (even by 10-100 times) in practical, porous electrodes. Since the diffusion within pores must be considered, a film diffusion coefficient was proposed to reflect the difference from bulk diffusion by a partition coefficient (partitioning between the bulk and the film formed on the pore walls) in a porous electrode system.[73] This difference existed on both sides making the results quantitatively comparable. We strongly recommend that these fundamental electrochemical measurements should be carried out using the actual electrode material that is intended to be used in the RFB. This will ensure that these measurements can actually serve as useful guides for RFB engineering. We measured the diffusion coefficients and rate constants on the same HT CF and CP that are also used as electrodes in the Ti-Ce RFBs and thus this measurement is much more representative of the conditions encountered in actual operation. The ECSA can be calculated from the double-layer capacitance[59]. The N-S equation itself has also been used calculate the ECSA, as long as an independent measure of the diffusion coefficient is available.[60] CVs of CP and HT CF were measured within non-Faradaic region to measure the double layer capacitance, C_{dl} (Figure

View Article Online
DOI: 10.1039/D5SE01171J

S2 and Table S2). With a geometrical surface area of 1 cm^2, the specific capacitance, C_s of HT CF was measured to be ~4700x that of CP. This improved C_s directly corelates to higher measured reaction rates over an electrode of the same geometric area even though the rate constant is unchanged. Based on the discussion above, the D_0 and k_0 numbers measured here can be defined as the "nominal" values because they accurately reflect the different effects of HT CF and CP with a common geometrical surface area. Similarly, the reaction rate constants listed in **Table 5** should be examined with this understanding of the effect of electrode surface area. Notably, the rate constant for Ce reduction was found to be lower than that for Ti oxidation while Ce oxidation was faster than Ti reduction. Thus, Ce was expected to be the rate limiting electrode during discharge while Ti was expected to be rate limiting during charge. To verify it, polarization curves of symmetric cells utilizing Ce or Ti electrolyte of 50% SOC were compared as depicted in Figure S3. The overpotential of Ce side was higher than Ti in discharge and vice versa in charge, which supported the finding that Ce was rate limiting during discharge and Ti during charge.

Table 5. Mass transfer and kinetics parameters of Ti & Ce reactions

Parameters	Ce_CP_a	Ce_CP_c	Ti_HT CF_a	Ti_HT CF_c
Diffusion coefficient D_0 ($x10^{-4}$ cm^2 s)	0.48 ± 0.04	0.58 ± 0.18	46.0 ± 6.2	105.1 ± 11.2
Standard reaction rate constant k_0 ($x10^{-4}$ cm s^{-1})	9.1 ± 0.5	6.5 ± 0.1	42.7 ± 3.5	3.8 ± 0.5

2.4 Ti-Ce RFBs performance

View Article Online
DOI: 10.1039/D5SE01171J

To verify the advantage of asymmetric electrode configuration, pristine CF and CP were used separately as positive electrodes in Ti-Ce RFBs to test the performance, depicted in **Figure 6**. Only positive electrodes were varied as the Ti electrolyte was found to not even wet the CP surface as shown in section 2.1. **Figure 6a** shows the performance at a relatively low current density (50 mA cm^{-2}) with different cycling durations. Over 10-minute cycles, the energy efficiency (EE) of CF was significantly higher than that of CP (85.6% vs. 76.0%) as the much higher active surface area of CF compared to than CP provided more active sites for the Ce reaction, thus promoting the reaction rate. However, as the cycling experiment proceeded, EE of CF and CP gradually decreased and increased respectively, and reached the same level in the 60-minute cycle stage (81.0%). As shown in **Figure S4**, the polarization losses of CF were gradually increased while that of CP remained constant. The degradation of CF during RFBs operation was consistent with the stability test in Ce(IV) electrolytes, i.e., the structure of CF was destroyed by the highly oxidizing nature of Ce(IV), leading to lower EE. On the contrary, it was interesting to find that since CP was resilient to Ce(IV), and EE of CP was promoted over time pointing to possible CP activation by Ce(IV) during the experiment to become more favorable for the Ce reaction. The difference in RFB performance between CF and CP was more significant at high current density (150 mA cm^{-2}), as shown in **Figure 6b**: the average EE of CF was only 48.6% while that of CP was 68.1%. Moreover, both EE and discharge capacity decreased over cycling when CF was used as the electrode of the Ce side. It is clearly shown in **Figure 6c** that the degradation of CF during cycling increased high frequency resistance (HFR) from 60 to 110 mOhm, while HFR of CP stayed under 30 mOhm. Higher HFR resulted in greater ohmic losses, which lowered the EE, especially when the applied current density was high. To identify the source of the increase in HFR on the untreated CF, characterization was performed on CP and CF at Ce side after cycling experiment. As shown

View Article Online
DOI: 10.1039/D5SE01171J

in Figure S5 (and compared to the SEM images in Figure 1), the surface morphology of CP was unchanged after cycling but CF showed significant surface roughening. The EDX results listed in Table S3 clearly show the dramatic increase (compared to CP) in surface oxygen on CF after cycling and this indicates that oxidative degradation of the untreated CF resulted in increasing charge transfer resistance and decreasing performance. Thus, CP was concluded to be the better choice of electrode for the Ce side, validating our choice based on CV measurements.

The generally accepted opinion about HFR in RFBs is that it is dominated by the ionic resistance of ion exchange membrane.[61-63] The contact resistance of other components in RFBs, especially that from porous CF, has been studied in some previous studies. A more compressed CF would result in a lower HFR, with possible destruction of the mechanical properties of CF and increase in pressure drop. The effect of compression ratio on this tradeoff was reported for VRFBs, with the optimum compression ratio lying within a wide range from 25% to 60%.[64-66] To identify the optimum compression ratio for CF on the Ti side, three different values (25%, 48%, and 53%) were selected based on the different types of gaskets during cell assembling, and the result is shown in **Figure S6**, Supporting Information. As the compression ratio was increased from 25% to 48%, the HFR decreased from 50 mOhm to 30 mOhm and correspondingly, EE increased from 63.5% to 67.7%. A further increase of compression ratio became difficult as CF tended to be broken, and the HFR from other components (e.g., membrane and electrolytes) remained unchanged. Our previous study utilized a hydraulic-electrical analogous model to reveal that when the compression was increased from 10 to 40%, the hydraulic power loss was promoted by approximately 40%.[74] The EE further increased to 69.2% when the compression ratio was increased to 53%, while the change of HFR was negligible, indicating that we had reached the HFR optimum. Based on this,

View Article Online
DOI: 10.1039/D5SE01171J

the compression ratio of HT CF on the Ti side should be kept at around 50% to yield the best performance.

The long-term cycling result with this optimal configuration (CP electrode on Ce side and 50% compressed HT CF electrode on the Ti side) over the entire SOC range is depicted in **Figure 7**. Notably, this optimization effort allowed us to increase the operating current density from 100 to 150 mA cm^{-2} over 100 cycles in 80 h, the average of coulombic efficiency and EE were 99.1% and 67.8% respectively, and about 93% of the initial discharge capacity was retained at the end of cycling. The cycling was conducted with a galvanostatic plus potentiostatic protocol, and some irreversible side reactions (e.g., hydrogen evolution) might happen when the cell was held at a high potential (2 V). The theoretically upper limit of charge capacity of the (n+1)th cycle was the same as discharge capacity of the nth cycle, which was lower than the charge capacity of the nth cycle due to the fact that the coulombic efficiency was close but never equal to 100%. Thereof, the discharge capacity would inevitably decrease overtime. Additionally, we observed almost no capacity fade over >200 cycles when the range of SOC over which we cycled was narrowed by imposing a time limit on the charge and discharge cycles as shown in **Figure S8**. The discharge voltage reached 1.4 V according to charge-discharge curves as depicted in **Figure S7**. The performance reported here is better than most other types of RFBs utilizing Ce, e.g., Zn-Ce,[67] Pb-Ce,[21] V-Ce RFBs,[22] and non-aqueous Ce RFBs[68] as summarized in **Table 6**. The operating current density of this work was the highest compared to previous studies, and a high current density is typically not beneficial to energy efficiency since the ohmic polarization is increased. Despite this, the energy efficiency of this work is still higher than most of previous studies. Furthermore, the concentration applied in this study is also the highest among all the studies, indicating a great advantage of promoting capacity storage and lowering capital cost. In a recent

View Article Online
DOI: 10.1039/D5SE01171J

study, the Ti compound was decorated on CF to enhance the kinetics of the Ce redox reaction, and a Fe-Ce RFB was developed based on this idea.[69] The EE from this study was 66.2% at 25 mA cm^{-2}, which was close to that of this study at 150 mA cm^{-2}. Thus, the Ti-Ce RFB presented here shows great potential for commercialization and scaling up.

Table 6. Comparison of Ce RFB performance between this work and previous studies

RFB type	Positive electrolyte	Negative electrolyte	Highest operating current density (mA cm^{-2})	Highest Discharge voltage (V)	EE (%)	# of finished cycles	Reference
Zn-Ce	0.8 M $Ce(CH_3SO_3)_3$ in 4 M MSA	1.5 M $Zn(CH_3SO_3)_2$ in 1 M MSA	50	1.77	59.3	57	[67]
Pb-Ce	1 M $Ce(CH_3SO_3)_3$ in 1 M MSA	1.5 M $Pb(CH_3SO_3)_2$ in 1 M MSA	10	1.67	79	800	[21]
V-Ce	0.9 M $Ce(CH_3SO_3)_3$ in 4 M MSA	0.9 M $VOSO_4$ in 5.8 M MSA	100	1.25	51	100	[22]
Non-aqueous V-Ce	0.05 M $[Ce(Py\text{-}O)_8][Tf_2N]_3$[a] in 0.5 M $TEABF_4$/ACN[b]	0.05 M $V(acac)_3$[c] in 0.5 M $TEABF_4$/ACN[b]	1	2.1	< 75	50	[68]
Fe-Ce	0.1 M $Ce(SO_4)_2$ in 1 M H_2SO_4	0.05 M $FeSO_4$ in 1 M H_2SO_4	25	0.8	66.2	100	[69]
Ti-Ce	0.9 M $Ce(CH_3SO_3)_3$ in 4 M MSA	0.9 M $TiOSO_4$ in 3.8 M MSA	150	1.4	67.8	100	This work

View Article Online
DOI: 10.1039/D5SE01171J

[a] cerium bis (trifuoromethylsulfonyl)imide; [b] tetraethylammonium tetrafluoroborate/acetonitrile; [c] vanadium acetylacetonate

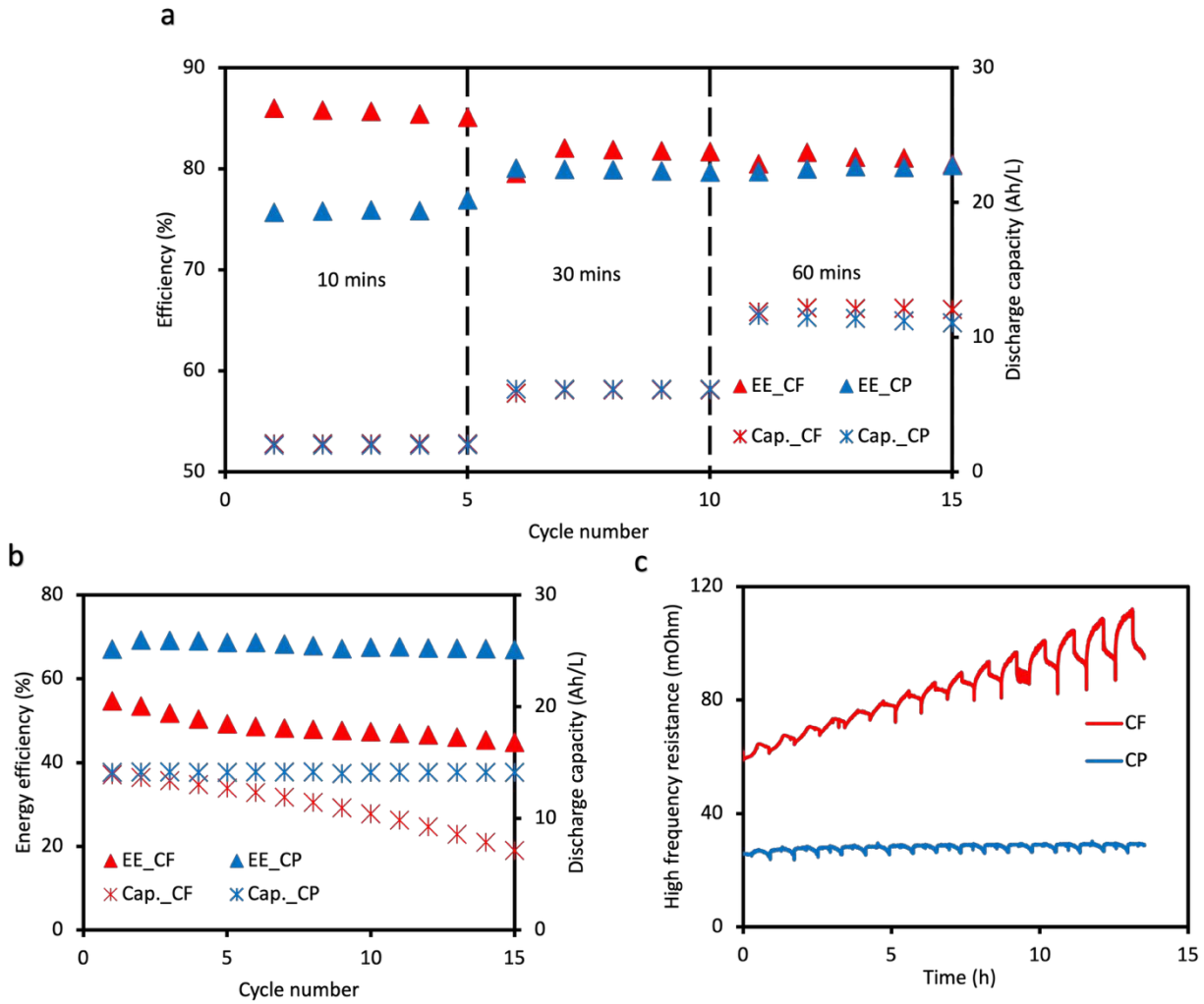

Figure 6. Ti-Ce RFB performance. Comparison between CF and CP working as electrodes of Ce side under a) galvanostatic 50 mA cm^{-2} with different charge/discharge durations and b) galvanostatic 150 mA cm^{-2} plus potentiostatic at 2/1 V for charge/discharge. c) HFR evolution comparison between CF and CP working as electrodes of Ce side with galvanostatic 150 mA cm^{-2} plus potentiostatic at 2/1 V for charge/discharge.

View Article Online
DOI: 10.1039/D5SE01171J

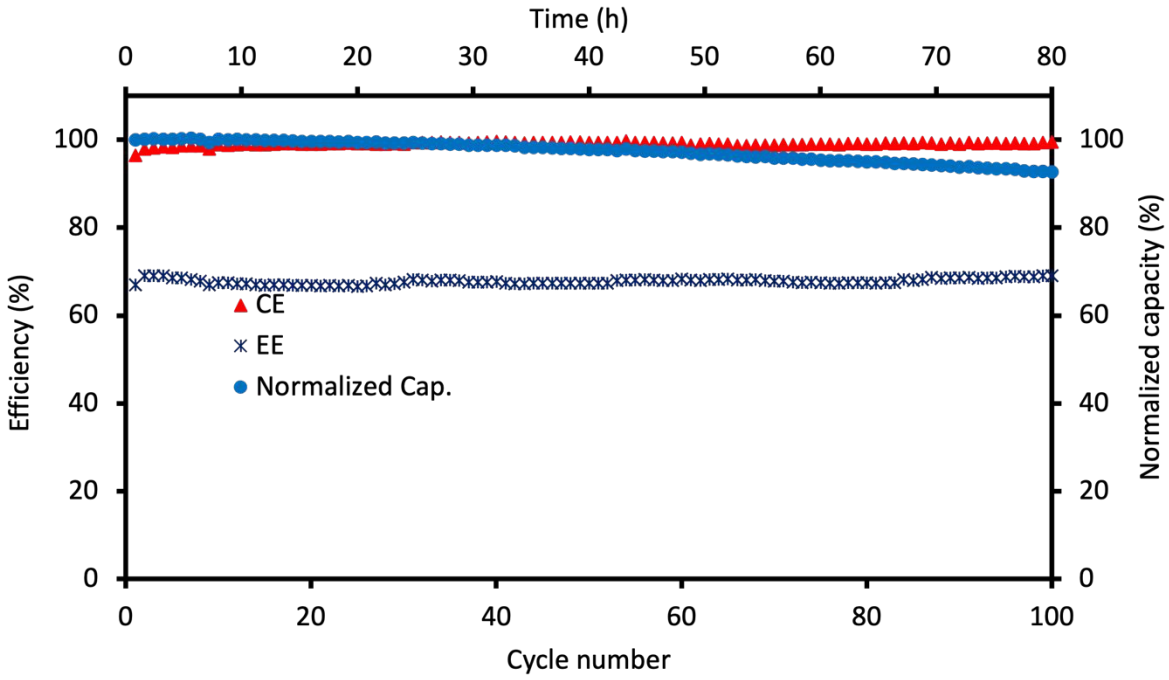

Figure 7. Long-term cycling performance of optimized RFB cell with CP/HT CF as the electrode of Ce/Ti side with galvanostatic 150 mA cm^{-2} plus potentiostatic at 2/1 V for charge/discharge.

Generalized design optimization approach for RFBs

During RFB operation, activation polarization, ohmic polarization, and concentration polarization is dominating respectively as current density increases, as shown in **Figure 8**. The overpotential induced by each type of polarization includes the contribution from both cathodic and anodic sides. For example, during discharge, Ce and Ti undergo cathodic and anodic reactions, respectively, and the activation polarization could be expressed as follows:

$$\eta_{act\_c} = \frac{RT}{\alpha_{Ce\_c}F} ln(i) - \frac{RT}{\alpha_{Ce\_c}F} ln(i_{0\_Ce}) \quad (7)$$

$$\eta_{act\_a} = \frac{RT}{\alpha_{Ti\_a}F} ln(i) - \frac{RT}{\alpha_{Ti\_a}F} ln(i_{0\_Ti}) \quad (8)$$

where i_0 is the exchange current density. Similarly, the ohmic overpotential could be expressed as

View Article Online
DOI: 10.1039/D5SE01171J

$$\eta_{ohmic\_c} = iA_{Ce}\frac{1}{G_{Ce}} \quad (9)$$

$$\eta_{ohmic\_a} = iA_{Ti}\frac{1}{G_{Ti}} \quad (10)$$

where A and G are electrode surface area and electrolyte conductance, respectively.

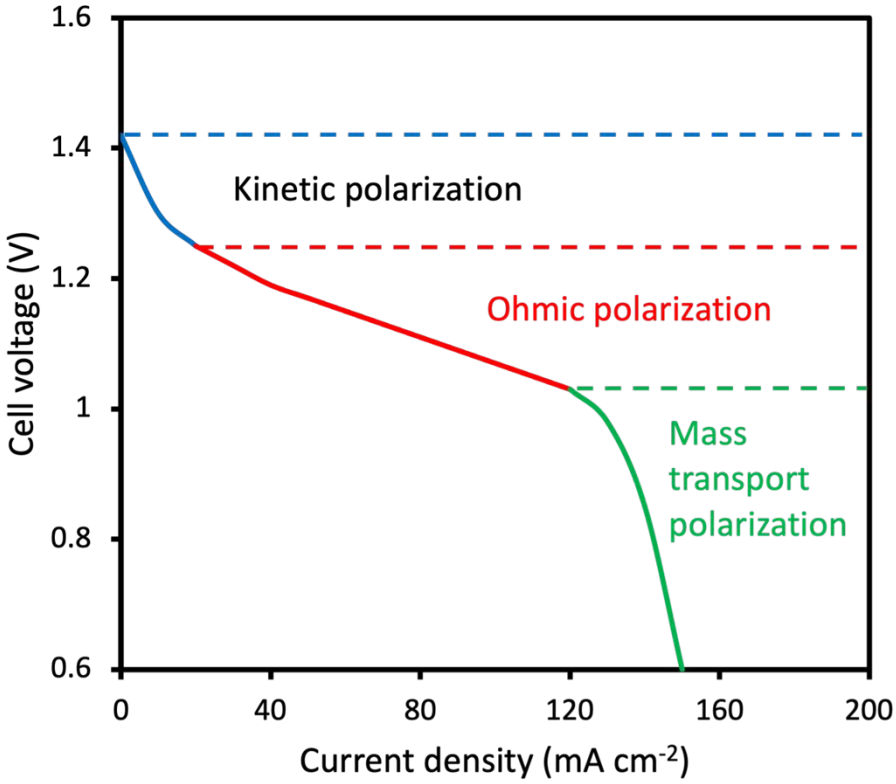

Figure 8. Illustration of polarization curve during RFB operation.

The polarization curve presented above is typical of RFBs and can be used as a general diagnostic tool to identify losses and areas for improvement. **Figure 9** depicts the interlinked RFB design parameters (e.g., electrode thickness, separator thickness etc.) and its effects on RFB performance parameters. **Table 7** provides suggested modifications to the RFB design depending on the performance limiting design parameter identified using the polarization curve.

View Article Online
DOI: 10.1039/D5SE01171J

469

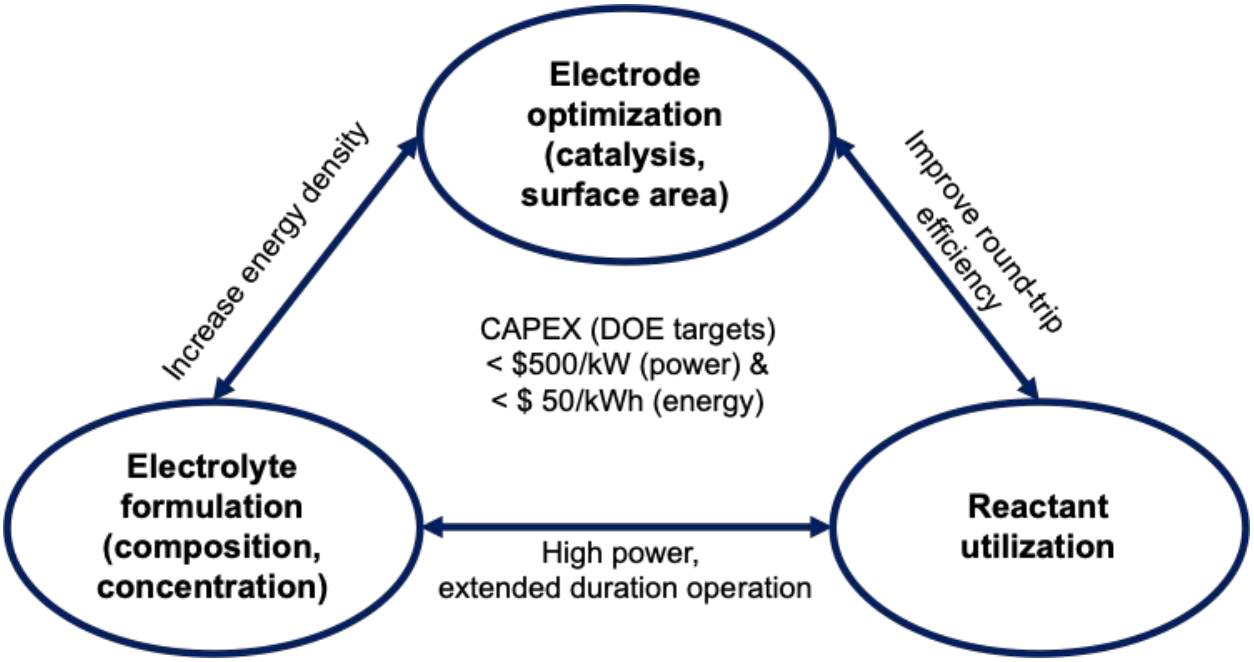

470

471 **Figure 9**. Interlinks between performance metrics and design parameters.

472 **Table 7**. Relationship matrix between RFB performance metrics and design paramters.

Affected performance parameter	RFB design variable	Governing equation and control variable	Design modifications examined
Energy efficiency (indirectly affected through RFB cell resistance)	1. Electrode thickness 2. Separator thickness 3. Electrolyte conductivity	1. $\sigma_{electrode} = \frac{\boldsymbol{t_{electrode}}}{R_{HFR}A_{electrode}}$ 2. $\sigma_{separator} = \frac{\boldsymbol{t_{separator}}}{R_{HFR}A_{separator}}$ 3. $\kappa_{electrolyte} = \frac{L}{R_{electrolyte}A} = z_+\nu_+\boldsymbol{C_{electrolyte}}(\boldsymbol{\lambda}_+ + \boldsymbol{\lambda}_-)$	1. Varying electrode thickness and porosity. 2. Thinner separator, reinforced separator. 3. Electrolyte additives, mixed supporting electrolytes.
Power density	1. Electrode surface area	1. $i = nF\boldsymbol{A}\boldsymbol{k}C$ 2. $k = \boldsymbol{k_0}\exp\left(-\frac{\alpha F\eta}{RT}\right)$	1. Varying electrode material and thickness. 2. Electrode pretreatment (thermal, H_3PO_4 immersion, *aqua regia*

View Article Online
DOI: 10.1039/D5SE01171J

	2. Electrode active surface modification		immersion) and/or Bi electrodeposition.

3. Conclusion

A Ti-Ce RFB with asymmetric electrode configuration was proposed and developed in this study guided by a series of broadly applicable fundamental surface- and electrochemical characterization techniques. It is shown that using the actual electrode and electrolyte employed in a RFB to also measure electrochemical characteristics like diffusion coefficient and rate constant leads to better agreement with cell level results and avoids the pitfalls introduced by idealized dilute electrolytes and model, non-porous, planar electrodes. Evaluating and downselecting electrode candidates based on surface wettability and electrochemical performance (reversibility, redox reaction rates), traditional, thermally treated CF was utilized as the negative electrode while CP was selected as the positive electrode as it was more resilient to the oxidizing nature of Ce(IV). This cell was further optimized by adjusting the CF compression ratio to balance reduced ohmic losses and increased pressure drop. This optimized RFB operated at 150 mA cm^{-2} and delivered a stable coulombic and energy efficiency of 99.1% and 67.8% respectively, and a capacity retention of 93% by the end of 100 cycles – a significant improvement across multiple metrics compared to other Ce-based RFBs. The demonstrated Ti-Ce RFB presents great potential for the development of economically and environmentally friendly inorganic RFBs. The approach presented herein can also be generalized to improve the performance of other RFBs.

4. Experimental section

View Article Online
DOI: 10.1039/D5SE01171J

Preparation of materials: Titanium oxysulfate ($TiOSO_4$) and MSA were purchased from Sigma-Aldrich; cerium carbonate ($Ce_2(CO_3)_3$) was purchased from Treibacher Industries A. G. Ti electrolyte was made by dissolving $TiOSO_4$ into deionized water first, then the corresponding amount of MSA was added; Ce electrolyte was made by mixing $Ce_2(CO_3)_3$ and deionized water to form a slurry first, then MSA was added slowly to react with $Ce_2(CO_3)_3$. The slurry was mixed by a magnetic bar rotated at a low speed (100 rpm). After every 1 mL of MSA was added, no more MSA was added until the reaction finished and no CO_2 bubbles were observed. CP (AvCarb MGL 190, Fuel Cell Store) and CF (GFA 6, SGL Group) were heat treated in a Muffle furnace at 500 °C for 8 h under an air atmosphere. The optimum treatment temperature was concluded based on a screening with different temperatures, as depicted in **Figure S10**. As the temperature increased from 400 to 550 °C, the EE first increased from 47.7% to 66.9% at 500 °C and then slightly decreased. The synthesis of quaternized cardo-poly(ether ketone)-based anion exchange membrane functionalized with trimethylamine (QPEK-C-TMA AEM) was the same as one of our previous studies.[70-71]

Electrochemical methods: Cyclic voltammetry (CV) was conducted with WaveNowXV Potentiostat Bundles (PINE Research), and a three-electrode system was set up utilizing an Ag/AgCl reference electrode, platinum wire counter electrode, and CP or CF working electrode. The geometrical surface area of the working electrode was 1 cm^2 for all tests. The scan range for Ti and Ce was -0.5 to 1 V and 0.8 to 1.9 V vs. Ag/AgCl, respectively, and four different scan rates, 1, 2.5, 5, and 10 mV/s were used for further calculation from N-S and K-K equations. The Ti and Ce electrolytes with 50% state of charge (SOC) were obtained by running a half-charge protocol in Ti-Ce RFB and then diluted 10 times using the same concentration of MSA on each side. The reason was that the current from the CV experiment would be extremely large with the original

View Article Online
DOI: 10.1039/D5SE01171J

concentration due to the much higher reaction activity of CP and CF compared with the more commonly used working electrode, glassy carbon, which would interfere with the identification of peak current position and value.

Characterization methods: SEM/EDX was conducted with an Environmental Scanning Electron Microscope (Thermofisher Quattro S ESEM) bundled with an Oxford AzTec Energy Dispersive X-Ray Spectrometer (EDXS). The acceleration voltage was 5 kV, and the working distance was around 10 mm. XPS was conducted with Physical Electronics 5000 VersaPhobe II Scanning ECSA Microprobe. A broad survey spectrum was finished before the fine scanning for each element. The contact angle picture was captured with a homemade goniometer mainly composed of a camera and lighting background, and the contact angle was then measured by ImageJ.

RFBs test: Ti-Ce RFBs were operated with an 857 Redox Flow Cell Test System (Scribner). The geometrical surface area of negative and positive electrodes was 25 cm^2 (5x5 cm). The volume of electrolyte on each side was 100 mL and it was pumped through the cell with a flow rate of 140 mL min^{-1}. The 50 mA cm^{-2} protocol was purely galvanostatic for both charge and discharge processes with different durations (10, 30, and 60 mins), and the battery was operated for 5 cycles under each time length. The 150 mA cm^{-2} protocol was galvanostatic plus potentiostatic to charge and discharge the system fully. In charge, the cell was applied at a current of 150 mA cm^{-2} until the potential reached the cutoff value (2 V), then the potential was held at this level until the current decreased to 20 mA cm^{-2}. Likewise, -150 mA cm^{-2} was applied at the beginning of discharge until the potential decreased to cutoff value (1 V), followed by a potentiostatic stage at this potential until the current increased to -20 mA cm^{-2}. The protocol for polarization curve could be found in section 2, Supporting Information.

View Article Online
DOI: 10.1039/D5SE01171J

Supporting Information Available

XPS survey data, Charge-discharge curves, Ti-Ce RFB performance with different CF compression ratio, properties of CP and CF available.

Funding Statement: This work was supported by the Advanced Research Projects Agency-Energy (ARPA-E), the US Department of Energy under award no. DE-AR0000768 as part of the Integration and Optimization of Novel Ion Conducting Solids (IONICS) program and the McKelvey School of Engineering, Washington University in St. Louis and the Roma B. & Raymond H. Wittcoff Distinguished University Professorship.

Acknowledgements: The authors would like to acknowledge the support of the Advanced Research Projects Agency-Energy (ARPA-E), the US Department of Energy under award no. DE-AR0000768 as part of the Integration and Optimization of Novel Ion Conducting Solids (IONICS) program and the McKelvey School of Engineering, Washington University in St. Louis and the Roma B. & Raymond H. Wittcoff Distinguished University Professorship. Jing Xie wants to thank Dr. Huafang Li from Institute of Materials Science & Engineering at Washington University in St. Louis for the help in terms of materials characterization.

Conflict of Interest Disclosure: The authors currently have no financial interests that may be perceived to influence the conclusions presented in this work. Some of the authors are seeking intellectual property protections on aspects of one or more technologies described in this report through the Office of Technology and Management (OTM) at Washington University in St. Louis (WUSTL).

View Article Online
DOI: 10.1039/D5SE01171J

560 **Data Availability Statement:** All of the data associated with these studies are represented in the
561 manuscript and supplemental information. The raw data are available from the corresponding
562 author upon reasonable request.

563

View Article Online
DOI: 10.1039/D5SE01171J

Reference list:

1. S. Chen, M. Zhang, P. Zou, B. Sun, and S. Tao, "Historical Development and Novel Concepts on Electrolytes for Aqueous Rechargeable Batteries." *Energy & Environmental Science* 15, no. 5 (January 1, 2022): 1805–39. https://doi.org/10.1039/d2ee00004k

2. K. Zou, W. Deng, Debbie S. Silvester, et al., "Carbonyl Chemistry for Advanced Electrochemical Energy Storage Systems." *ACS Nano* 18, no. 31 (July 29, 2024): 19950–0. https://doi.org/10.1021/acsnano.4c02307

3. Y. Liang, H. Dong, D. Aurbach, and Y. Yao, "Current Status and Future Directions of Multivalent Metal-ion Batteries." *Nature Energy* 5, no. 9 (July 16, 2020): 646–56. https://doi.org/10.1038/s41560-020-0655-0

4. M. Lin, M. Gong, B. Lu, et al., "An Ultrafast Rechargeable Aluminium-ion Battery." *Nature* 520, no. 7547 (April 1, 2015): 324–28. https://doi.org/10.1038/nature14340

5. B. Li, Z. Nie, M. Vijayakumar, et al., "Ambipolar Zinc-Polyiodide Electrolyte for a High-Energy Density Aqueous Redox Flow Battery." *Nature Communications* 6, no. 1 (February 24, 2015): 6303. https://doi.org/10.1038/ncomms7303

6. A. Hollas, X. Wei, V. Murugesan, et al., "A Biomimetic High-capacity Phenazine-based Anolyte for Aqueous Organic Redox Flow Batteries." *Nature Energy* 3, no. 6 (May 30, 2018): 508–14. https://doi.org/10.1038/s41560-018-0167-3

7. Z. Li, and Y. Lu, "Polysulfide-based Redox Flow Batteries With Long Life and Low Levelized Cost Enabled by Charge-reinforced Ion-selective Membranes." *Nature Energy* 6, no. 5 (April 1, 2021): 517–28. https://doi.org/10.1038/s41560-021-00804-x

8. M. Rychcik, and M. Skyllas-Kazacos, "Characteristics of a New All-vanadium Redox Flow Battery." *Journal of Power Sources* 22, no. 1 (January 1, 1988): 59–67. https://doi.org/10.1016/0378-7753(88)80005-3

View Article Online
DOI: 10.1039/D5SE01171J

9. H.R. Jiang, J. Sun, L. Wei, M.C. Wu, W. Shyy, and T.S. Zhao, "A High Power Density and Long Cycle Life Vanadium Redox Flow Battery." *Energy Storage Materials* 24 (July 6, 2019): 529–40. https://doi.org/10.1016/j.ensm.2019.07.005

10. K.E. Rodby, R.L. Jaffe, E.A. Olivetti, and F.R. Brushett, "Materials Availability and Supply Chain Considerations for Vanadium in Grid-scale Redox Flow Batteries." *Journal of Power Sources* 560 (January 19, 2023): 232605. https://doi.org/10.1016/j.jpowsour.2022.232605

11. L. Tang, P. Leung, M.R. Mohamed, et al., "Capital Cost Evaluation of Conventional and Emerging Redox Flow Batteries for Grid Storage Applications." *Electrochimica Acta* 437 (January 2023): 141460. https://doi.org/10.1016/j.electacta.2022.141460

12. R.M. Darling, K.G. Gallagher, J.A. Kowalski, S. Ha, and F.R. Brushett, "Pathways to Low-Cost Electrochemical Energy Storage: A Comparison of Aqueous and Nonaqueous Flow Batteries." *Energy Environmental Science* 7, no. 11 (September 16, 2014): 3459–77. https://doi.org/10.1039/C4EE02158D

13. R.M. Darling, "Techno-Economic Analyses of Several Redox Flow Batteries Using Levelized Cost of Energy Storage." *Current Opinion in Chemical Engineering* 37 (September 2022): 100855. https://doi.org/10.1016/j.coche.2022.100855

14. S. Sankarasubramanian, and V. Ramani, Redox flow battery, *US Patent* 11,177,497, 2021.

15. S. Sankarasubramanian, Y. Zhang, C. He, T. Gregory, and V. Ramani, "An Aqueous, Electrode-Decoupled Redox-Flow Battery for Long Duration Energy Storage." *Preprint* January 27, 2021. https://doi.org/10.21203/rs.3.rs-150474/v1.

16. K. Binnemans, P.T. Jones, K. Van Acker, B. Blanpain, B. Mishra, and D. Apelian, "Rare-Earth Economics: The Balance Problem." *JOM* 65, no. 7 (July 2013): 846–48. https://doi.org/10.1007/s11837-013-0639-7

17. H. Tsurugi, and K. Mashima, "Renaissance of Homogeneous Cerium Catalysts with Unique Ce(IV/III) Couple: Redox-Mediated Organic Transformations Involving Homolysis of Ce(IV)–Ligand Covalent Bonds." *Journal of the American Chemical Society* 143, no. 21 (June 2, 2021): 7879–90. https://doi.org/10.1021/jacs.1c02889

View Article Online
DOI: 10.1039/D5SE01171J

18. A. Paulenova, S.E. Creager, J.D. Navratil, and Y. Wei, "Redox Potentials and Kinetics of the Ce3+/Ce4+ Redox Reaction and Solubility of Cerium Sulfates in Sulfuric Acid Solutions." *Journal of Power Sources* 109, no. 2 (July 2002): 431–38. https://doi.org/10.1016/S0378-7753(02)00109-X

19. R.M. Spotnitz, R.P. Kreh, J.T. Lundquist, and P.J. Press, "Mediated Electrosynthesis with Cerium (IV) in Methanesulphonic Acid." *Journal of Applied Electrochemistry* 20, no. 2 (March 1990): 209–15. https://doi.org/10.1007/BF01033596

20. P.K. Leung, C. Ponce-de-León, F.J. Recio, P. Herrasti, and F.C. Walsh, "Corrosion of the Zinc Negative Electrode of Zinc–Cerium Hybrid Redox Flow Batteries in Methanesulfonic Acid." *Journal of Applied Electrochemistry* 44, no. 9 (September 2014): 1025–35. https://doi.org/10.1007/s10800-014-0714-y

21. Z. Na, S. Xu, D. Yin, and L. Wang, "A Cerium–Lead Redox Flow Battery System Employing Supporting Electrolyte of Methanesulfonic Acid." *Journal of Power Sources* 295 (November 2015): 28–32. https://doi.org/10.1016/j.jpowsour.2015.06.115

22. S. Sankarasubramanian, Y. Zhang, and V. Ramani, "Methanesulfonic Acid-Based Electrode-Decoupled Vanadium–Cerium Redox Flow Battery Exhibits Significantly Improved Capacity and Cycle Life," *Sustainable Energy & Fuels* 3, no. 9 (2019): 2417–25. https://doi.org/10.1039/C9SE00286C

23. M. Sarraf, E.R. Ghomi, S. Alipour, S. Ramakrishna, and N.L Sukiman, "A State-of-the-Art Review of the Fabrication and Characteristics of Titanium and Its Alloys for Biomedical Applications." *Bio-Design and Manufacturing* 5, no. 2 (April 2022): 371–95. https://doi.org/10.1007/s42242-021-00170-3

24. V. Anil Kumar, R.K. Gupta, M.J.N.V. Prasad, and S.V.S. Narayana Murty, "Recent Advances in Processing of Titanium Alloys and Titanium Aluminides for Space Applications: A Review." *Journal of Materials Research* 36, no. 3 (February 15, 2021): 689–716. https://doi.org/10.1557/s43578-021-00104-w

25. P. Pushp, S.M. Dasharath, and C. Arati, "Classification and Applications of Titanium and Its Alloys." *Materials Today: Proceedings* 54 (2022): 537–42. https://doi.org/10.1016/j.matpr.2022.01.008

26. C. Yang, H. Wang, S. Lu, et al., "Titanium Nitride as an Electrocatalyst for V(II)/V(III) Redox Couples in All-Vanadium Redox Flow Batteries." *Electrochimica Acta* 182 (November 2015): 834–40. https://doi.org/10.1016/j.electacta.2015.09.155

View Article Online
DOI: 10.1039/D5SE01171J

27. L. Zhang, Y. Jiang, H. Wang, P. Qian, J. Sheng, and H. Shi, "Sulfonated Poly (Ether Ketone)/Sulfonated Titanium Dioxide Hybrid Membrane with High Selectivity and Good Stability for Vanadium Redox Flow Battery." *Journal of Energy Storage* 45 (January 2022): 103705. https://doi.org/10.1016/j.est.2021.103705

28. S.I.U. Ahmed, M. Shahid, and S. Sankarasubramanian, "Aqueous Titanium Redox Flow Batteries—State-of-the-Art and Future Potential." *Frontiers in Energy Research* 10 (October 10, 2022): 1021201. https://doi.org/10.3389/fenrg.2022.1021201

29. L. Qiao, M. Fang, S. Liu, H. Zhang, and X. Ma, "New-Generation Iron–Titanium Flow Batteries with Low Cost and Ultrahigh Stability for Stationary Energy Storage." *Chemical Engineering Journal* 434 (April 2022): 134588. https://doi.org/10.1016/j.cej.2022.134588

30. M. Nan, M. Wu, Y. Liu, L. Qiao, H. Zhang, and X. Ma, "Boosting the Areal Capacity of Titanium-Manganese Single Flow Battery by Fe^{2+} /Fe^{3+} Redox Mediator." *Small Methods* 7, no. 1 (January 2023): 2201266. https://doi.org/10.1002/smtd.202201266

31. W.H. Wang, and X.D. Wang, "Investigation of Ir-Modified Carbon Felt as the Positive Electrode of an All-Vanadium Redox Flow Battery." *Electrochimica Acta* 52, no. 24 (August 2007): 6755–62. https://doi.org/10.1016/j.electacta.2007.04.121

32. Z. He, Y. Jiang, Y. Li, et al., "Carbon Layer-Exfoliated, Wettability-Enhanced, SO_3H-Functionalized Carbon Paper: A Superior Positive Electrode for Vanadium Redox Flow Battery." *Carbon* 127 (February 2018): 297–304. https://doi.org/10.1016/j.carbon.2017.11.006

33. B. Sun, and M. Skyllas-Kazacos, "Modification of Graphite Electrode Materials for Vanadium Redox Flow Battery Application—I. Thermal Treatment." *Electrochimica Acta* 37, no. 7 (June 1992): 1253–60. https://doi.org/10.1016/0013-4686(92)85064-R

34. K.V. Greco, A. Forner-Cuenca, A. Mularczyk, J. Eller, and F.R. Brushett, "Elucidating the Nuanced Effects of Thermal Pretreatment on Carbon Paper Electrodes for Vanadium Redox Flow Batteries." *ACS Applied Materials & Interfaces* 10, no. 51 (December 26, 2018): 44430–42. https://doi.org/10.1021/acsami.8b15793

View Article Online
DOI: 10.1039/D5SE01171J

699 35. E. Agar, C.R. Dennison, K.W. Knehr, and E.C. Kumbur, "Identification of Performance Limiting
700 Electrode Using Asymmetric Cell Configuration in Vanadium Redox Flow Batteries." *Journal of Power*
701 *Sources* 225 (March 2013): 89–94. https://doi.org/10.1016/j.jpowsour.2012.10.016

702

703 36. Y. Li, J. Parrondo, S. Sankarasubramanian, and V. Ramani, "Impact of Surface Carbonyl- and
704 Hydroxyl-Group Concentrations on Electrode Kinetics in an All-Vanadium Redox Flow Battery." *The*
705 *Journal of Physical Chemistry C* 123, no. 11 (March 21, 2019): 6370–78.
706 https://doi.org/10.1021/acs.jpcc.8b11874

707

708 37. G. Wei, X. Fan, J. Liu, and C Yan, "Electrospun Carbon Nanofibers/Electrocatalyst Hybrids as
709 Asymmetric Electrodes for Vanadium Re.dox Flow Battery." *Journal of Power Sources* 281 (May 2015):
710 1–6. https://doi.org/10.1016/j.jpowsour.2015.01.161

711

712 38. M. Jing, A. Zhang, N. Liu, et al., "Asymmetric Batteries Based on Customized Positive and Negative
713 Electrodes-an Effective Strategy to Further Improve the Performance of Vanadium Redox Flow Batteries."
714 *Electrochimica Acta* 473 (January 2024): 143478. https://doi.org/10.1016/j.electacta.2023.143478

715

716 39. M.Y. Lu, W.W. Yang, X.S. Bai, Y.M. Deng, and Y.L. He, "Performance Improvement of a Vanadium
717 Redox Flow Battery with Asymmetric Electrode Designs." *Electrochimica Acta* 319 (October 2019): 210–
718 26. https://doi.org/10.1016/j.electacta.2019.06.158

719

720 40. P. Mazúr, J. Mrlík, J. Beneš, et al., "Performance Evaluation of Thermally Treated Graphite Felt
721 Electrodes for Vanadium Redox Flow Battery and Their Four-Point Single Cell Characterization." *Journal*
722 *of Power Sources* 380 (March 2018): 105–14. https://doi.org/10.1016/j.jpowsour.2018.01.079

723

724 41. J. Xu, Y. Zhang, Z. Huang, C. Jia, and S. Wang, "Surface Modification of Carbon-Based Electrodes for
725 Vanadium Redox Flow Batteries." *Energy & Fuels* 35, no. 10 (May 20, 2021): 8617–33.
726 https://doi.org/10.1021/acs.energyfuels.1c00722

727

728 42. G. Nikiforidis, Y. Xiang, and W.A. Daoud, "Electrochemical Behavior of Carbon Paper on Cerium
729 Methanesulfonate Electrolytes for Zinc-Cerium Flow Battery." *Electrochimica Acta* 157 (March 2015):
730 274–81. https://doi.org/10.1016/j.electacta.2014.11.134

731

View Article Online
DOI: 10.1039/D5SE01171J

732 43. A. Kaur, K.I. Jeong, S.S. Kim, and J.W. Lim, "Optimization of Thermal Treatment of Carbon Felt
733 Electrode Based on the Mechanical Properties for High-Efficiency Vanadium Redox Flow Batteries."
734 *Composite Structures* 290 (June 2022): 115546. https://doi.org/10.1016/j.compstruct.2022.115546

735

736 44. H. Lim, M. Shin, C. Noh, E. Koo, Y. Kwon, and K.Y. Chung, "Performance Evaluation of Aqueous
737 All Iron Redox Flow Batteries Using Heat Treated Graphite Felt Electrode." *Korean Journal of Chemical*
738 *Engineering* 39, no. 11 (November 2022): 3146–54. https://doi.org/10.1007/s11814-022-1195-z

739

740 45. G. Nikiforidis, and W.A. Daoud, "Thermally Modified Graphite Electrodes for the Positive Side of the
741 Zinc-Cerium Redox Flow Battery." *Journal of The Electrochemical Society* 162, no. 6 (2015): A809–19.
742 https://doi.org/10.1149/2.0041506jes

743

744 46. L. Faggiano, G. Lacarbonara, W.D. Badenhorst, L. Murtomäki, L. Sanz, and C. Arbizzani, "Short
745 Thermal Treatment of Carbon Felts for Copper-Based Redox Flow Batteries." *Journal of Power Sources*
746 520 (February 2022): 230846. https://doi.org/10.1016/j.jpowsour.2021.230846

747

748 47. A.J. Bard, and L.R. Faulkner, *Electrochemical Methods: Fundamentals and Applications*. 2nd ed.. New
749 York Weinheim: Wiley, 2000

750

751 48. H. Dong, J. Chen, L. Feng, W. Zhang, X. Guan, and T.J. Strathmann, "Degradation of Organic
752 Contaminants through Activating Bisulfite by Cerium(IV): A Sulfate Radical-Predominant Oxidation
753 Process." *Chemical Engineering Journal* 357 (February 2019): 328–36.
754 https://doi.org/10.1016/j.cej.2018.09.024

755

756 49. R.S. Nicholson, and I. Shain, "Theory of Stationary Electrode Polarography. Single Scan and Cyclic
757 Methods Applied to Reversible, Irreversible, and Kinetic Systems." *Analytical Chemistry* 36, no. 4 (April
758 1, 1964): 706–23. https://doi.org/10.1021/ac60210a007

759

760 50. R.S. Nicholson, "Theory and Application of Cyclic Voltammetry for Measurement of Electrode
761 Reaction Kinetics." *Analytical Chemistry* 37, no. 11 (October 1, 1965): 1351–55.
762 https://doi.org/10.1021/ac60230a016

763

764 51. R.J. Klingler, and J.K. Kochi, "Electron-Transfer Kinetics from Cyclic Voltammetry. Quantitative
765 Description of Electrochemical Reversibility." *The Journal of Physical Chemistry* 85, no. 12 (June 1981):
766 1731–41. https://doi.org/10.1021/j150612a028

767

View Article Online
DOI: 10.1039/D5SE01171J

52. T. Herr, P. Fischer, J. Tübke, K. Pinkwart, and P. Elsner, "Increasing the Energy Density of the Non-Aqueous Vanadium Redox Flow Battery with the Acetonitrile-1,3-Dioxolane–Dimethyl Sulfoxide Solvent Mixture." *Journal of Power Sources* 265 (November 2014): 317–24. https://doi.org/10.1016/j.jpowsour.2014.04.141

53. I. Gunasekara, M.N. Ates, S. Mukerjee, E.J. Plichta, M.A. Hendrickson, and K.M. Abraham, "Solid Phase FePC Catalysts for Increased Stability of Oxygen Reduction Reaction Intermediates at the Cathode/Electrolyte Interface in Lithium Air Batteries." *Journal of The Electrochemical Society* 164, no. 4 (2017): A760–69. https://doi.org/10.1149/2.1221704jes

54. Z. Masood, H. Muhammad, and I.A. Tahiri. "Comparison of Different Electrochemical Methodologies for Electrode Reactions: A Case Study of Paracetamol." *Electrochem* 5, no. 1 (January 31, 2024): 57–69. https://doi.org/10.3390/electrochem5010004

55. J.H. Savéant, and D. Tessier, "Variation of the Electrochemical Transfer Coefficient with Potential." *Faraday Discussions of the Chemical Society* 74, no. 0 (1982): 57–72. https://doi.org/10.1039/DC9827400057

56. E.J.F. Dickinson, and A.J. Wain, "The Butler-Volmer Equation in Electrochemical Theory: Origins, Value, and Practical Application." *Journal of Electroanalytical Chemistry* 872 (September 2020): 114145. https://doi.org/10.1016/j.jelechem.2020.114145

57. J.M. Nzikou, M. Aurousseau, and F. Lapicque, "Electrochemical Investigations of the Ce(III)/Ce(IV) Couple Related to a Ce(IV)-Assisted Process for SO_2/NO_x Abatement." *Journal of Applied Electrochemistry* 25, no. 10 (October 1995). https://doi.org/10.1007/BF00241592

58. Z. Xie, D. Zhou, F. Xiong, S. Zhang, and K. Huang, "Cerium-Zinc Redox Flow Battery: Positive Half-Cell Electrolyte Studies." *Journal of Rare Earths* 29, no. 6 (June 2011): 567–73. https://doi.org/10.1016/S1002-0721(10)60499-1

59. Y. Gao, H. Wang, Q. Ma, et al., "Carbon Sheet-Decorated Graphite Felt Electrode with High Catalytic Activity for Vanadium Redox Flow Batteries." *Carbon* 148 (July 2019): 9–15. https://doi.org/10.1016/j.carbon.2019.03.035

60. D.O. Opar, R. Nankya, J. Lee, and H. Jung, "Assessment of Three-Dimensional Nitrogen-Doped Mesoporous Graphene Functionalized Carbon Felt Electrodes for High-Performance All Vanadium Redox Flow Batteries." *Applied Surface Science* 531 (November 2020): 147391. https://doi.org/10.1016/j.apsusc.2020.147391

View Article Online
DOI: 10.1039/D5SE01171J

807 61. Y.A. Gandomi, D.S. Aaron, J.R. Houser, et al., "Critical Review—Experimental Diagnostics and
808 Material Characterization Techniques Used on Redox Flow Batteries." *Journal of The Electrochemical*
809 *Society* 165, no. 5 (2018): A970–1010. https://doi.org/10.1149/2.0601805jes

810

811 62. T.C. Chang, J.P. Zhang, and Y.K. Fuh, "Electrical, Mechanical and Morphological Properties of
812 Compressed Carbon Felt Electrodes in Vanadium Redox Flow Battery." *Journal of Power Sources* 245
813 (January 2014): 66–75. https://doi.org/10.1016/j.jpowsour.2013.06.018

814

815 63. P. Bai, and M.Z. Bazant, "Performance and Degradation of A Lithium-Bromine Rechargeable Fuel Cell
816 Using Highly Concentrated Catholytes." *Electrochimica Acta* 202 (June 2016): 216–23.
817 https://doi.org/10.1016/j.electacta.2016.04.010

818

819 64. P.C. Ghimire, A. Bhattarai, R. Schweiss, G.G. Scherer, N. Wai, and Q. Yan, "A Comprehensive Study
820 of Electrode Compression Effects in All Vanadium Redox Flow Batteries Including Locally Resolved
821 Measurements." *Applied Energy* 230 (November 2018): 974–82.
822 https://doi.org/10.1016/j.apenergy.2018.09.049

823

824 65. J. Charvát, P. Mazúr, J. Dundálek, et al., "Performance Enhancement of Vanadium Redox Flow Battery
825 by Optimized Electrode Compression and Operational Conditions." *Journal of Energy Storage* 30 (August
826 2020): 101468. https://doi.org/10.1016/j.est.2020.101468

827

828 66. R. Gundlapalli, and S. Jayanti, "Effect of Electrode Compression and Operating Parameters on the
829 Performance of Large Vanadium Redox Flow Battery Cells." *Journal of Power Sources* 427 (July 2019):
830 231–42. https://doi.org/10.1016/j.jpowsour.2019.04.059

831

832 67. P.K. Leung, C. Ponce-de-León, C.T.J. Low, A.A. Shah, and F.C. Walsh, "Characterization of a Zinc–
833 Cerium Flow Battery." *Journal of Power Sources* 196, no. 11 (June 2011): 5174–85.
834 https://doi.org/10.1016/j.jpowsour.2011.01.095

835

836 68. Y. Li, P. Geysens, X. Zhang, et al., "Cerium-Containing Complexes for Low-Cost, Non-Aqueous Redox
837 Flow Batteries (RFBs)." *Journal of Power Sources* 450 (February 2020): 227634.
838 https://doi.org/10.1016/j.jpowsour.2019.227634

839

840 69. J. Wu, X. Cao, Y. Ji, et al., "Boosting Kinetics of Ce^{3+} /Ce^{4+} Redox Reaction by Constructing TiC/TiO2
841 Heterojunction for Cerium‐Based Flow Batteries." *Advanced Functional Materials* 34, no. 3 (January
842 2024): 2309825. https://doi.org/10.1002/adfm.202309825

843

View Article Online
DOI: 10.1039/D5SE01171J

844 70. S. Yun, J. Parrondo, and V. Ramani, "Derivatized Cardo-Polyetherketone Anion Exchange Membranes
845 for All-Vanadium Redox Flow Batteries." *Journal of Materials Chemistry A* 2, no. 18 (2014): 6605–15.
846 https://doi.org/10.1039/C4TA00166D

847

848 71. S. Yun, J. Parrondo, and V. Ramani. "Composite Anion Exchange Membranes Based on Quaternized
849 Cardo-Poly(Etherketone) and Quaternized Inorganic Fillers for Vanadium Redox Flow Battery
850 Applications." *International Journal of Hydrogen Energy* 41, no. 25 (July 2016): 10766–75.
851 https://doi.org/10.1016/j.ijhydene.2016.04.060

852

853 72. S.I.U. Ahmed, and S. Sankarasubramanian. "Low pH Titanium Electrochemistry in the Presence
854 of Sulfuric Acid and Its Implications for Redox Flow Battery Applications." *Journal of The*
855 *Electrochemical Society* 171, no. 6 (2024): 060538. https://doi.org/10.1149/1945-7111/ad5975.

856

857 73. J. Seo, S. Sankarasubramanian, N. Singh, F. Mizuno, K. Takechi, and Jai Prakash. "Effect of
858 Cathode Porosity on the Lithium-Air Cell Oxygen Reduction Reaction – A Rotating Ring-Disk
859 Electrode Investigation." *Electrochimica Acta* 248 (September 2017): 570–77.
860 https://doi.org/10.1016/j.electacta.2017.07.121.

861

862 74. E. Asadipour, and V. K. Ramani. "A Computationally-cost Effective Model for Fluid Flow in
863 Redox Flow Batteries. " *AIChE Journal* 69, no. 7 (2023): e18051.
864 https://doi.org/10.1002/aic.18051.

View Article Online
DOI: 10.1039/D5SE01171J

Data Availability Statement: All of the data associated with these studies are represented in the manuscript and supplemental information. The raw data are available from the corresponding author upon reasonable request.